Complex oxide nanomembranes for energy conversion and storage: A review

Kian Kerman[a] and Shriram Ramanathan
Materials Science Group in Applied Physics, Harvard School of Engineering and Applied Sciences, Cambridge, Massachusetts 02138

(Received 19 May 2013; accepted 24 September 2013)

Oxide membranes are the foundation of several electrochemical devices and sensors, where functionality is related to selective transport of electrons and ions through a membrane or physical responses from an external perturbation. The ability to engineer power sources and sensors for the rapidly growing field of autonomous systems requires high power density and specific energy. Clamped free-standing nanoscale membranes provide an experimentally tunable platform to explore the limits of dimensionality reduction for such purposes. This review addresses the following: (i) advancing experimental methods to fabricate nanoscale oxide membranes that can sustain a chemical potential gradient, thermomechanically stable under large thermal cycles, and can be electrically interrogated with negligible parasitic loss; (ii) a representative example of high performance energy devices, solid oxide fuel cells, utilizing such membranes; and (iii) a brief discussion on emerging research directions broadly in the areas of condensed matter sciences and energy conversion and storage intersecting low-dimensional complex oxide materials.

I. INTRODUCTION

Membranes that possess selective transport properties are ubiquitous in everyday life, from inorganic devices such as batteries to biological ion channels in cell walls. Though vastly different in purpose, the underlying mechanism of operation is strikingly similar. The membrane serves to separate regions of dissimilar chemical potentials and allows selective permeation of a particular species that determines the overall functionality. In this review, we will focus on the emerging field of complex oxide nanomembranes having thicknesses in the range of 10–100 nm, with particular emphasis on their use in the context of energy conversion devices. We discuss fabrication challenges and complexities involved in forming stable suspended oxide membranes and representative enabling device technologies. The oxygen ion conducting electrolyte is used as a case study in the framework of an energy conversion device, namely thin film solid oxide fuel cells (TF-SOFCs), to exemplify specific advances in device fabrication and testing, but the ideology presented is widely pertinent to many oxide material systems. Figure 1 illustrates some oxide materials that have been realized as nanomembranes to date, grouped by respective functionality.[1–11] It is tremendously challenging to fabricate oxide membranes due to their inherent brittleness and the sensitivity of electronic properties to subtle composition changes such as cation or anion nonstoichiometry. The motivation for reducing dimensionality of these materials is linked to three main aspects: (A) exploring the ultimate limits of material functionality, (B) reduction of losses related to oxide separator components at the nanoscale, and (C) exploration of the interplay between science, engineering, and manufacturing for societally relevant technologies.

A. Fundamental oxide material considerations

Figure 2 presents some of the length scales and physical phenomena of interest.[12] Of note is that two-dimensional crossover in complex oxides is not necessarily at the monolayer scale. Induced space charge potentials can be a function of dopant concentration, temperature, and oxygen partial pressure.[13] The profile of carriers is significantly influenced at length scales on the order of tens of nanometers. The fundamental limitations of thickness reduction for a separation membrane can be related to the ability to selectively conduct, described by the transference number, $t_i = \frac{\sigma_i}{\sigma_i+\sigma_e}$, where σ_i and σ_e represent ionic and electronic conductivity, respectively. For example, consider the oxide electrolyte that must have electronic insulating properties in conjunction with selective ionic conduction, $t_i = 1$. In ultrathin films, the characteristic sample length can approach the Debye length (λ) which is expressed by, $\lambda = \sqrt{\frac{\varepsilon\varepsilon_0 kT}{2F^2z^2C}}$, where $\varepsilon\varepsilon_0$ is the dielectric permittivity, k is the universal gas constant, T is the absolute temperature, F is the Faraday's constant, z is the charge of the ionic

[a]Address all correspondence to this author.
e-mail: kkerman@fas.harvard.edu
DOI: 10.1557/jmr.2013.301

 © Materials Research Society 2013

https://doi.org/10.1557/jmr.2013.301 Published online by Cambridge University Press

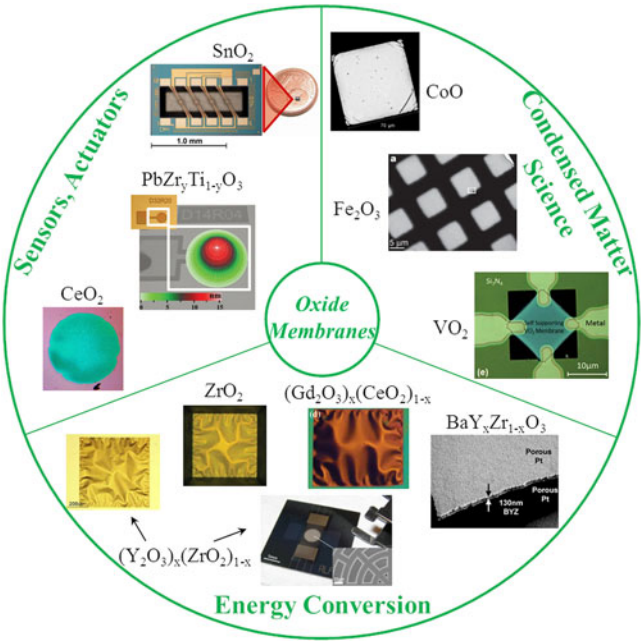


FIG. 1. A brief survey of complex oxide nanomembranes with applications in sensors and actuators, energy conversion, and condensed matter science is shown. While there is overlap with the applications of many of these materials, they are grouped to demonstrate the versatility that complex oxides possess. Within sensors and actuators, a fully fabricated metal-oxide (MOX) sensing module with SnO_2,[1] piezoelectric $Pb(ZryTi_{1-y})O_3$ for micro-electromechanical systems (MEMS) systems,[2] and CeO_2 as an oxygen conductor or strain sensor.[3] Within energy conversion, ZrO_2 for oxygen conduction in thin film fuel cells or oxygen sensors,[4] large area YSZ membrane for transport studies,[5] an integrated YSZ membrane for a TF-SOFC,[6] mixed conducting CGO for TF-SOFCs or chemical strain sensors,[7] and proton-conducting $BaY_{0.2}Zr_{0.8}O_3$ application in fuel cells.[8] Within condensed matter science, a monolayer of CoO produced by self-assembly for nanosieves,[9] self-assembled Fe_2O_3 for meta-materials,[10] and VO_2 for low power switching.[11] All figures have been reprinted with permission from respective publishers.

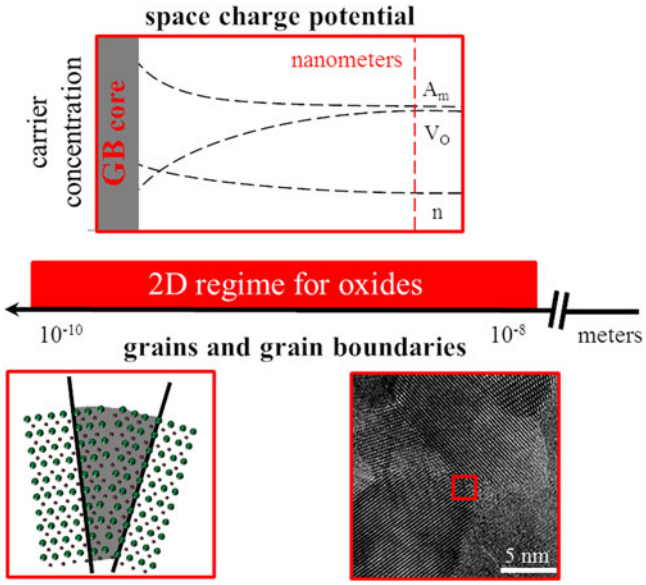


FIG. 2. The common length scales discussed in this review and pertinent to complex oxide membranes in general. A generic carrier concentration profile for aliovalently doped oxides shows how singly charged acceptors (A_m), doubly charged oxygen vacancies (V_O), and electronic carriers (n) can vary spatially in regions on the order of tens of nanometers away from a grain boundary core. A representative transmission electron micrograph of polycrystalline YSZ[12] and a schematic of a grain boundary are also shown. Micrograph used with permission.

species, and C is the bulk concentration of the majority carrier. λ is typically on the order of tens of nanometers, which can be comparable to film thicknesses in membranes. Two-dimensional effects such as anomalous inversion can set in at or below this length scale. In some cases, this is defined by an alternate dimension such as the electrical boundary width in an internal interface; for example, a grain boundary. Having such phenomena on similar length scales modifies the boundary conditions of Poisson's equation and can therefore have nontrivial effects on the carrier concentration profile as shown schematically in Fig. 2.[14,15] λ can be considerably altered in aliovalently doped oxides, where the Mott–Schottky approximation is valid,[16] and as such, every case must be both theoretically and experimentally considered individually.

Oxide heterostructures could have local regions of heterogeneous charge distribution leading to anomalous conduction behavior. Polycrystalline films have an inherent space charge region, originating from local areas of electrostatic charge such as grain boundary cores. A nonuniform chemical profile must exist in the near vicinity of such regions to maintain electrochemical neutrality.[17] Nanocrystalline materials, such as many of the thin films described herein, may have grain sizes that approach λ. This may result in substantially different transport properties of nanostructured films compared to bulk counterparts. For example, a significant research effort evaluating the effects of thickness scaling on films bound to a substrate, which is also related to film strain, on σ_i in the $(Y_2O_3)_x(ZrO_2)_{1-x}$ (YSZ) system has resulted in alternative observations of enhanced[18–21] and reduced[22–25] σ_i. With regard to grain size reduction, it is generally accepted that the grain boundaries of ZrO_2 and CeO_2 based electrolytes are positive.[26–28] Therefore, decreasing grain size in these systems should lead to a decrease in σ_i and increase in electronic conductivity, which has been corroborated for YSZ.[29]

Oxide films in the sub-100 nm thickness range also present chemical complexity in that dopant segregation can play an increasingly significant role in the optimal conductivity and phase stability. Early work on the enhancement of σ_i in YSZ and CeO_2 thin films hinted at the difference in stoichiometry between nanocrystalline films and their bulk counterparts.[30] Recent studies have shown that σ_i of $(Gd_2O_3)_x(CeO_2)_{1-x}$ (CGO) thin films with thickness comparable to grain size (20 nm) is over four times higher than that of bulk and can be attributed to reduction of grain boundary resistance in conjunction with Gd dopant segregation.[31] Dopant distribution in CGO, and hence the transport behavior, has been shown to be largely influenced

https://doi.org/10.1557/jmr.2013.301 Published online by Cambridge University Press

by annealing conditions in controlled oxygen partial pressures.[32] Molecular dynamics simulations show that the conductivity of YSZ can increase two orders of magnitude at ultralow thicknesses (3–9 nm) due to dopant segregation at the film–substrate interface.[33] An enhancement of σ_i in YSZ films (1000-nm thickness) having a grain size in the range of 30–50 nm was observed at unexpectedly low Y_2O_3 doping concentrations, ascribed to the extension of the cubic phase below equilibrium doping levels expected from the bulk phase diagram due to nanocrystalline grain structure.[34] It is noted here that most studies have been conducted with in-plane geometry on thin films bound to a substrate. Studies on suspended membranes could lead to unambiguous conclusions on the nature of charge conduction at these length scales. For example, Garbayo et al.[5] have characterized the out-of-plane conductivity of YSZ membranes noting that σ_i was similar to that of bulk for film thicknesses in the range of 60–240 nm, though comparable films on a substrate were an order of magnitude lower. Fabrication and transport measurements on suspended oxide nanomembranes are an elegant way to probe some of the aforementioned scientific challenges but require significant experimental effort.

B. Electrochemical potential separation and membrane considerations

In electrochemical devices that utilize two electrodes separated by an electrolyte component, there are three main losses, one of which is associated ionic transport across the electrolyte.[35] In the case of oxygen conduction, the oxygen flux per unit area can be expressed by $j = \sigma_i \frac{d\varphi}{dx}$, where $\frac{d\varphi}{dx}$ represents linear voltage gradient across the electrolyte, respectively.[36] In the limit $\frac{d\varphi}{dx} = \frac{\varphi}{h}$, where φ is the cell voltage and h is the electrolyte thickness, it can be deduced that the resistance takes a form similar to Ohm's law and is directly proportional to h. As a result, reducing the electrolyte thickness can effectively minimize transport loss through the separator. This formalism assumes that there is equivalent electrochemical activity across the surface of the electrodes, which is often not the case in heterogeneous porous electrodes. However, this assumption serves as a bound for discussion and motivation for the experimental work described herein.

As discussed in Sec. I. A, the effects of dimensionality and grain size can be understood through characteristic length scales such as λ; however, the influence of strain is not as straightforward and requires the consideration of multiple contributions, including local lattice distortion. In an effort to explain the origins of interface-induced enhancements of σ_i in ultrathin films, several theoretical works have emerged. First principle studies have indicated that oxygen diffusivity can increase up to a critical tensile strain and revealed that there are competing lattice strain and local bonding components of importance for macroscopic transport.[37,38] A recent experimental investigation of epitaxial YSZ has corroborated the former studies, showing an enhanced σ_i, with decreased activation energy for films below 15 nm.[39] Work on CeO_2 based materials has highlighted the importance of how processing routes can be a strong factor in determining lattice strain and thus, the effects on σ_i.[40] Further, recent work on CeO_2 and YSZ has shown the coexistence of amorphous and crystalline materials in some nanostructured films processed by spray pyrolysis,[41,42] which can hinder transport properties if not adequately considered during processing.

C. Synergistic benefits of membrane structures

Oxide membranes have the potential to provide insight into the aforementioned subjects as a robust tunable experimental platform. Structures made with oxide materials having a wide variety of applications are ripe for exploration across chemistry, physics, materials science, mechanics, and engineering. The ability to probe such structures requires detailed transport expertise, while new models to describe the behavior of the aforementioned physical phenomena require the cooperation of rigorous experimental and theoretical efforts. Figure 3 presents a schematic illustration of the various property relationships that can be probed using membrane structures described in this review.

The remainder of this review is organized into three sections focused on (II) membrane fabrication methods and design considerations; (III) a case study of energy conversion devices, TF-SOFCs, utilizing oxide membrane electrolytes; and (IV) future research directions and possibilities for oxide membranes.

II. FABRICATION OF SUSPENDED OXIDE MEMBRANES

The creation of a useful self-supported oxide membrane is a significant experimental challenge which can

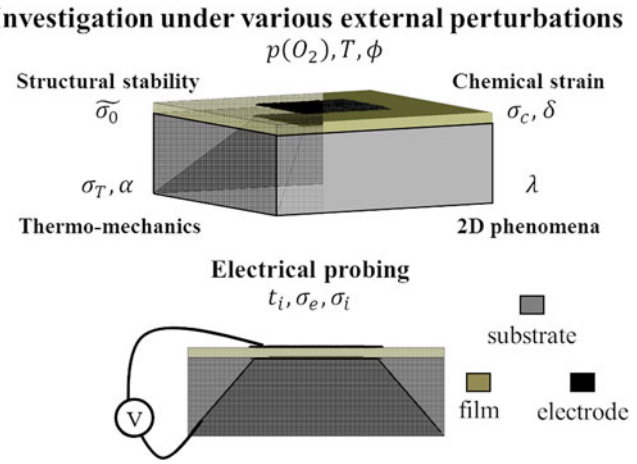


FIG. 3. A schematic example of the complex material research interplay described in this review, with symbols described in detail throughout the text.

https://doi.org/10.1557/jmr.2013.301 Published online by Cambridge University Press

be approached by two main techniques: (A) chemical and (B) physical. The complexity and issues associated with electrical probing of suspended membranes are discussed in Sec. III.

A. Chemical approaches to membrane fabrication

Chemical approaches utilize a transfer process to span the thin film material over an opening or grid, whereas physical methods remove an underlying support layer to release the membrane. The former routes can be achieved using a Langmuir–Blodgett (LB) technique to transfer a film to a patterned substrate.[43] The LB technique utilizes a group of amphiphilic molecules that arrange to minimize surface energy, forming an ultrathin film at a liquid/air interface. This film can then be transferred to an arbitrary substrate by pulling vertically through the monolayer, assuming that the wetting characteristics are well known.[44] Some oxide membranes, such as graphene-oxide and Fe_2O_3,[9,10,45] have been fabricated in this way. Simple solution-based techniques, such as vacuum filtration explored in graphene oxide,[46] may also play a significant role in cost-effective fabrication of membranes. There are many other chemical approaches to forming ultrathin films for membrane applications,[47] however, the majority of techniques have not found utility for oxide materials and therefore their use remains limited in the context of this review.

B. Physical approaches to membrane fabrication

Utilizing a physical method typically involves the growth of a film on a patterned substrate followed by several selective etch steps to form the self-supported membrane. Oxide film growth can be carried out using a plethora of techniques that classify broadly into physical vapor deposition (PVD), chemical vapor deposition (CVD), and atomic layer deposition (ALD). These methods have been discussed recently in the perspective of oxide materials utilized for TF-SOFCs.[48,49] There are numerous factors influencing the choice of deposition process, but the end result, in the context of forming oxide membranes, is equivalent. A generic schematic outline of the membrane processing steps is depicted in Fig. 4. The method is broadly applicable provided the etch characteristics of a given substrate are established and can be used in a vast number of material systems. It should be noted that there are specific concerns, requiring due diligence to achieve pristine membranes. We will discuss this aspect in two central subcategories of (C) substrate etching and micromachining and (D) mechanics of suspended membranes.

C. Etching

Unlike much of the research described previously utilizing films on substrates, electrically interconnected

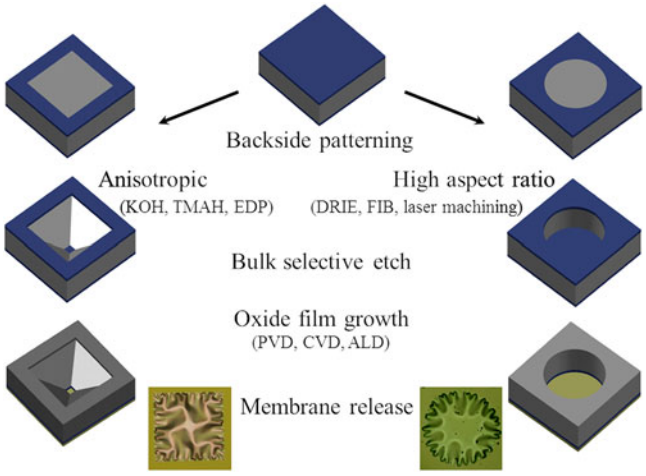


FIG. 4. An illustration of the physical procedure for producing oxide membranes on an easily etched substrate using conventional semiconductor processing techniques is shown. A barrier layer is needed on both sides of the substrate for pattern transfer and bulk micromachining, respectively. This backside is patterned using a lithographic technique and subsequently selectively etched to reveal the desired feature on the front side of the substrate. After the oxide film is deposited, the final support is etched away, creating a self-supported clamped membrane. Two schematic illustrations are shown and described in the text as anisotropic and high aspect ratio etches. A representative optical micrograph of a released YSZ oxide nanomembrane is shown for each case with a square of side length 160 μm and a circle of diameter 100 μm.[50]

membrane development requires significant microfabrication processing. Etching of the underlying substrate poses several complexities, such as geometric constriction, contamination, and postdeposition film stability. For example, in Si some common wet etchants used are potassium hydroxide (KOH), tetramethyl ammonium hydroxide (TMAH), or ethylene-diamine-pyrocatechol water (EDP).[51–54] These solutions etch in an anisotropic manner, meaning that there is a significantly higher etch rate along certain crystallographic directions. There is an abundance of data on KOH and it is widely used in microelectromechanical systems (MEMS).[53,54] KOH has a selectivity, the ratio of etching rates along different directions, of up to 1:400 for (111)/(100). Therefore, when using this substrate–etchant combination, the geometric membrane design inherently possesses straight edges and hence, corners. Many self-supported YSZ membranes and TF-SOFCs fabricated to date have used this approach[5,55–59]; though a stress concentrator, such as a corner, is not traditionally desired. An anisotropic etch greatly hinders the active membrane area utilized per substrate. For example, fabricating a square membrane of side length 200 μm on a 500-μm-thick (100) Si substrate using KOH necessitates a square of side length 908 μm be patterned on the backside, leading to approximately 22% surface area utilization, defined as $\frac{\text{Area}_{\text{membrane}}}{\text{Area}_{\text{patterned}}}$, not accounting for unused substrate area, which would further lower

https://doi.org/10.1557/jmr.2013.301 Published online by Cambridge University Press

utilization. This aspect can be significantly improved as the membrane area is sizably scaled, though other stability and processing issues arise and additional support layers are necessary.[60] Nevertheless, KOH is often used due to its low cost and fast etch rates. An additional benefit, not explored or discussed to date, is the possibility of generating H_2 during microfabrication processes that could later be used as fuel in TF-SOFCs or other electrochemical devices. KOH etches Si through the following reaction[61]; $Si + 2OH^- + 2H_2O \rightarrow SiO_2(OH)_2^{2-} + 2H_2$. Therefore, if evolved H_2 gas was captured and stored during the processing of energy devices or MEMS, there could be a synergistic relationship between manufacturing and energy production. For example, KOH etching of an array of square membranes from a 500-μm-thick Si wafer having a diameter of 100 mm would result in the production of a few cubic centimeters of H_2. Taking this to an industrial scale, i.e., thousands of wafers processed per day, indicates that this may be a feasible potential venture depending on capital costs.

An alternative to the commonly used anisotropic etchants described above are isotropic agents such as HF, which we will not discuss in detail as it typically etches oxide materials rendering it difficult to use, but there have been explorations into its feasibility for particular substrate film combinations.[62,63] In contrast, high aspect ratio micromachining can be achieved using methods such as deep reactive ion etching (DRIE), laser micromachining, focused ion beam (FIB), or powder blasting.[53,54] While these methods are more costly and time consuming than the aforementioned anisotropic wet etches, they can lead to very high surface area utilizations. YSZ membranes for TF-SOFCs have been fabricated using DRIE processing.[6] Corrugated oxide membranes, which have a larger projected geometric area than the actual patterned area, can also be made using a combination of DRIE and KOH techniques or nano-sphere lithography for TF-SOFC applications.[64–66] Other less common substrates, such as glass, have been micromachined using some of the aforementioned techniques to fabricate oxide membranes for use in TF-SOFCs.[67]

Once the micromachining has been carried out and the oxide film has been grown, the membrane must be released. This is achieved by removing the etch-stop, which in the case of Si, is typically SiO_2 or Si_3N_4 since they possess slow etch rates in the previously described mediums. These barriers are removed by plasma etching using a combination of CF_4, SF_6, and O_2 gases.[53,54] During processing, the oxide film is passively exposed to the plasma environment and when the barrier layer is fully removed, the oxide is directly exposed. Therefore, the impact of these species on the physical properties of oxide films, such as surface morphology, film thickness, microstructure, and conductivity should be considered when developing processing schemes to fabricate oxide membranes. For oxygen conducting materials used in TF-SOFCs, such as YSZ and CGO, these final etches appear to have negligible effects.[5,56,58,63] The well-known oxide etching characteristics of HF has detrimental effects on CGO,[63] rendering it impractical for many oxide film processes. Substrate specific contamination must also be considered. For example, Si contamination plays a vital role in the electrode kinetics and oxygen incorporation at the surface of YSZ, which necessitates carefully controlled fabrication.[68] Further, significant migration (11 at.%) of Si to the surface of YSZ films grown on Si_3N_4/Si substrates has been observed at annealing temperatures of 1000 °C, whereas only trace amounts (1 at.%) were detected for samples annealed at 600 °C.[69] Of course, as described previously, using ultrathin YSZ membranes enables the lowering of operating temperatures in TF-SOFCs, moving device temperatures away from this potential degradation mechanism.

D. Mechanics of suspended membranes

Deposition of the oxide film that will constitute the membrane is arguably the most important aspect of the fabrication process for numerous reasons, discussed below. Although the implementation and creation of robust oxide membranes are in their infancy, there is much to be gained from previous work in solid mechanics. The fundamental physical aspects of buckling in mechanically clamped membranes, often referred to as thin plates, is a well-studied problem.[70–74] For square membranes, buckling deformations can be characterized by a scaled stress parameter; $\widetilde{\sigma_0} = \frac{\sigma_0}{E}\left(\frac{L}{h}\right)^2$, where σ_0, E, L, and h represent the residual stress, elastic modulus, side length, and thickness of the film assuming a constant value of Poisson's ratio. This result follows from a rescaling of the von Karman energy function and can be modified for arbitrary geometries using a similar formalism.[71] Material selection dictates E, but other parameters are externally controllable, though not necessarily independent. In polycrystalline films, σ_0 can be a result of atomic peening and thermally induced stress during growth, whereas in epitaxial films, σ_0 is largely related to the substrate–film lattice parameter mismatch.[75] For polycrystalline YSZ grown by radio frequency (RF) sputtering, σ_0 as a function of h is shown in Fig. 5(a).[76] The relaxation of the initial peening induced σ_0 at larger film thicknesses is a result of crystallite coalescence, also referred to as grain growth.[75,82,83] It can be deduced that there is interplay between deposition conditions, which can control σ_0, film thickness, and influence transport properties of the oxide film. Previous work on square micromachined membranes has outlined that buckling begins at $\widetilde{\sigma_0} \sim 10^2$ and that stable elastic configurations appear at $\widetilde{\sigma_0} \sim 10^3$.[72,76]

Deposition technique, conditions, and postprocessing can strongly influence the microstructure, crystalline quality, texture, and subsequently, σ_0 of oxide films.

https://doi.org/10.1557/jmr.2013.301 Published online by Cambridge University Press

Consequently, when designing an ultrathin oxide membrane, the region of stability using $\widetilde{\sigma_0}$ remains valid, though the mechanisms by which it is achieved may differ depending on deposition techniques. A survey of σ_0 as a function of film thickness for YSZ films grown by various techniques is plotted in Fig. 5(b),[5,76–81] showing the large spread of values for different film processing procedures on various substrates. Of particular note is that even the sign of the measured stress can be altered depending on the deposition technique. This is of extraordinary importance, indicating that individual film processing techniques and physical structures must be well described and characterized to produce robust membranes. For example, a systematic in situ study of the stress evolution of YSZ grown on Si by RF sputtering indicates that deposition rate is a key component in the steady state film stress, with larger compressive stresses appearing at slower deposition rates.[84] This study does not take the significant aspect of growth stoppage and subsequent relaxation into account.[83] It also presents a constant stress value as a function of thickness up to 175 nm,[84] confirming that postprocessing is of great significance when attempting to engineer $\widetilde{\sigma_0}$ for stable membranes. Though we do not highlight growth pressure, deposition bias, or other key controllable aspects during film growth in Fig. 5(b), they are crucial parameters for as-deposited film stress and should be methodically studied for any prospective deposition process. This has been shown in brief for YSZ films.[80,85] Figure 6(a) depicts an example temperature–pressure schematic of the microstructures obtained in YSZ and CGO films grown by pulsed laser deposition (PLD),[86] illustrating that some of the microscopic complexity arising from film deposition must be addressed when attempting to form a stable oxide membrane. Recent work on the crystallization of

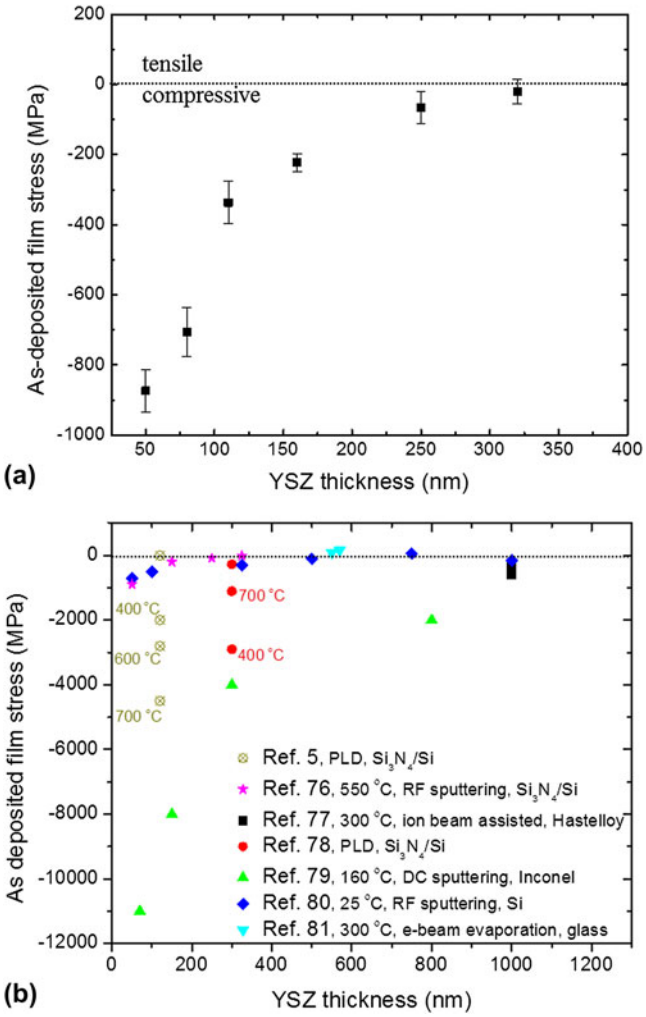


FIG. 5. The complexities of film deposition techniques on σ_0 for polycrystalline YSZ with various dopant concentration, but all of cubic crystal structure; (a) thickness dependence of σ_0 on RF sputtered YSZ deposited at 550 °C from an oxide target in 4.5 mTorr Ar on Si_3N_4/Si substrates[76]; (b) an example of the various reported values of as-deposited film stress for YSZ using different PVD deposition techniques and substrates highlighting the importance of specific processes used during membrane fabrication.[5,76–81]

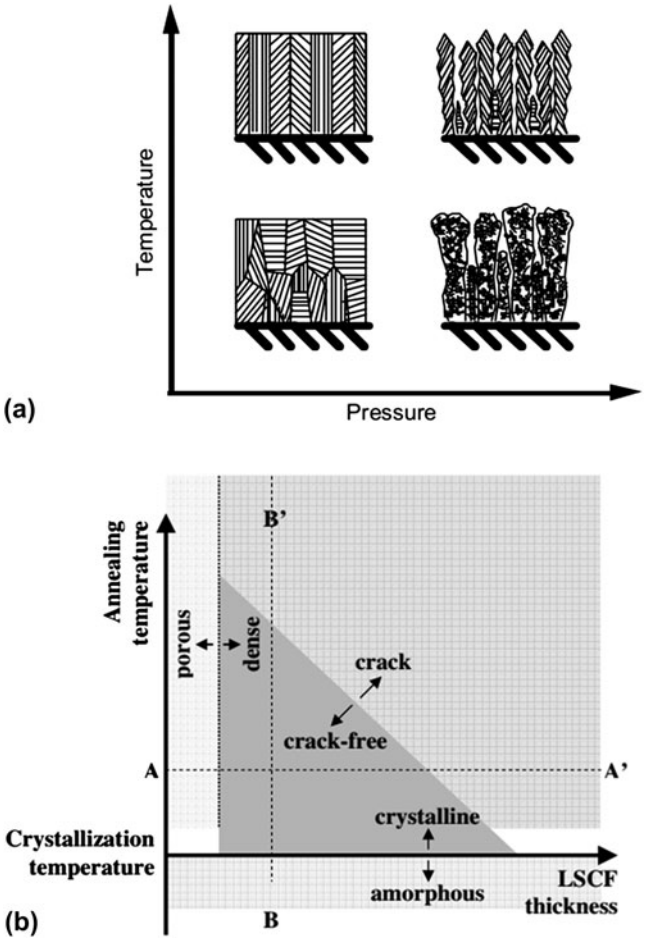


FIG. 6. The effect of processing on microstructure: (a) a schematic illustration of the microstructural variation in YSZ and CGO films as a function of temperature and pressure[86] and (b) an example post-processing diagram for LSCF thin films illustrating the complexity of engineering multiple oxides into a stable membrane structure.[87] Images are used with permission.

https://doi.org/10.1557/jmr.2013.301 Published online by Cambridge University Press

YSZ films grown by PLD has highlighted how postannealing can determine microstructure, phase purity, and microstrain,[88] which are of importance for film integration.

As described previously, microstructure such as grain size, shape, and orientation can have profound effects on transport properties. In the case of TF-SOFCs, a defect-free, gas tight YSZ membrane is necessary to maintain a potential difference; therefore any microstructural cracks or pinholes compromise the device efficiency. This aspect will be discussed in Sec. III but warrants consideration in the context of fabrication since great effort has been dedicated to making pin-hole free single layer, bilayer, and even trilayer oxide heterostructure membranes.[87,89–94] When multiple dense oxide layers are desired in membrane form, the film deposition and postprocessing aspect is far more convoluted. Significant work on the postdeposition processing for sputtered films in the $La_xSr_{1-x}Co_yFe_{1-y}O_3$ (LSCF)/YSZ self-supported membrane system has been undertaken by Lai et al.[87,92] A representative processing space for LSCF thin films is depicted in Fig. 6(b) and has been used to produce a robust manufacturing process for oxide heterostructure membranes for TF-SOFCs up to several millimeters in side length.[87]

In addition to σ_0, thermally induced strain, σ_T, must be considered for membranes operating with a nonzero change in temperature ($\Delta T > 0$). For a substrate and film having different linear coefficients of expansion, $\sigma_T = \int_{T_1}^{T_2} \frac{(\alpha_f - \alpha_s)E_f}{1-\upsilon_f} dT$.[82] Here α_f and α_s represent the linear expansion coefficients of the film and the substrate, respectively and $\frac{E_f}{1-\upsilon_f}$ the biaxial modulus of the film. If $\alpha_f \neq \alpha_s$, an additional tensile or compressive stress is generated when $|\Delta T| > 0$, which implies that careful optimization of σ_0 is required to counteract an induced tensile fracture. This can occur in the event of $\sigma_T > 0$ by classic tensile rupture or in the event of $\sigma_T < 0$ by causing larger buckling deformations, in turn forming higher tensile bending stresses, potentially leading to failure. In the case of TF-SOFCs, the membrane fracture could lead to fuel air mixing, which has serious safety implications. Therefore, adequate material design and thin film engineering are necessary for robust membranes resistant to many thermal cycles and other external perturbations. In addition to σ_T, the fabrication of complex oxide membranes undergoing a structural phase transition within the desired operating temperature requires knowledge of local lattice changes. A recent investigation on VO_2 membranes elucidated that tensile stress associated with the metal–insulator phase transition led to spontaneous cracking which was accompanied by local twinning, signifying stress-induced plastic behavior.[95] In fact, this tendency limited early research efforts on vanadium dioxide as domains could be permanently altered by the induced stress caused by the phase transition.[96] Nonetheless, vanadium oxide anodes have been successfully utilized in self-supported oxide membrane energy conversion and storage devices that are thermomechanically stable.[97]

Complex oxides possess a unique nonstoichiometry induced stress discussed here as chemical stress, σ_c (also referred to as "chemical strain" in the literature).[3,98–103] σ_c arises due to the fact that oxide crystals can exist with partially incomplete anion stoichiometry, the deviation frequently represented as δ. A recent theoretical study discussed the origins of σ_c being related to the formation of oxygen vacancies and the resulting cation radius change, which lead to respective lattice changes.[101] In the context of complex oxide membranes, σ_c must be adequately understood for a particular material system as well as fabrication process. For example, anomalous expansion of $CeO_{2-\delta}$ materials at room temperature has been shown to lead to membrane instabilities over time.[3,104] In the context of TF-SOFCs, the construction of CGO–YSZ oxide alloys attempted to overcome some of the chemomechanical restraints of a material having large σ_c.[50] A recent study on the addition of ZrO_2 to $CeO_{2-\delta}$ has shown promise for reducing σ_c,[102] possibly overcoming some of the additional mechanical challenges associated with chemical stress limiting the use of high σ_i materials in membrane form. Additional information on the complexity and nature of σ_c can be found in the literature.[103,105,106]

One of the crucial aspects toward the usage of oxide membranes is scalability. Despite the aforementioned challenges, Fig. 7 illustrates some of the triumphs in geometric scaling of YSZ membranes to date utilizing various unique approaches.[60,65] Grid-supported circular membranes having diameters up to five mm have also been fabricated.[6] Another method leveraging a gel-supported technique was successful in fabricating square membranes with edge lengths up to five millimeters.[107] Additional studies and investigations into the multifaceted nature of thermo-chemical-mechanical coupling in complex oxides is required to extend these auspicious initial results to a wider range of functional oxide materials. Similarly, a Weibull-type study on the failure statistics of fabricated membranes merits detailed investigation to supplement initial stress considerations.[76,78]

III. THIN FILM SOLID OXIDE FUEL CELLS

Integrating thin film electrolytes for fuel cells has long been considered a worthy goal.[108,109] We discuss state of the art and challenging aspects of membrane integration by exploring (A) proof-of-concept energy conversion devices, (B) electrode challenges, and (C) new functionalities enabled by membrane technology.

A. Proof-of-concept thin film fuel cells with nanoscale electrolyte membranes

The motivation for using ultrathin oxide membranes for electrolytes in TF-SOFCs arises naturally since it

https://doi.org/10.1557/jmr.2013.301 Published online by Cambridge University Press

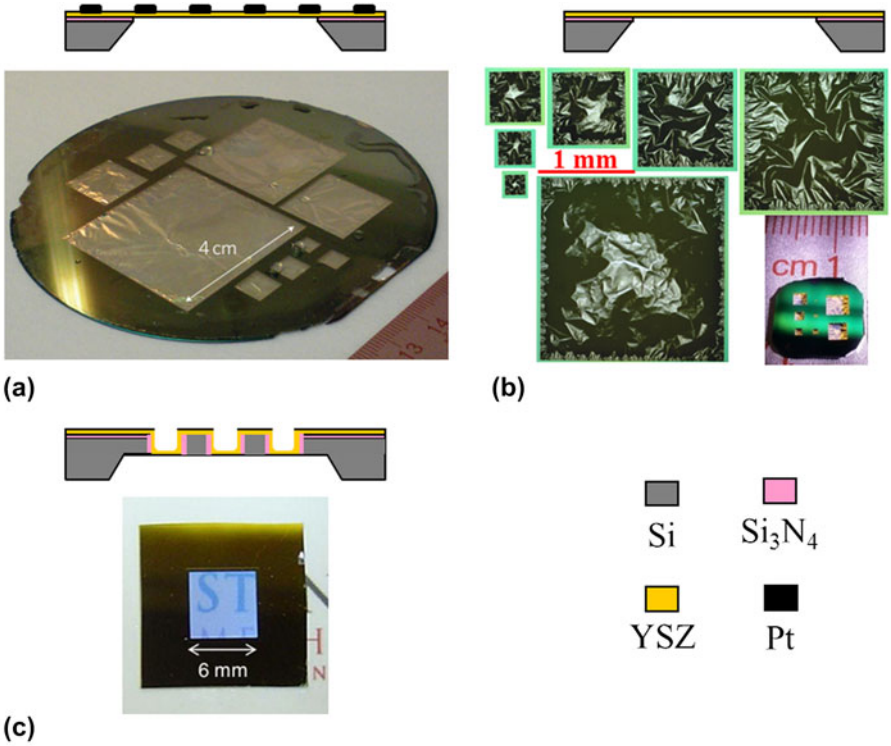


FIG. 7. The scalability of oxide membranes with YSZ thin films using three distinct techniques, namely grid support, stress control, and corrugation; (a) a grid supported design with membranes spanning several millimeters in side length,[60] (b) free-standing YSZ membranes with tuned internal film stress to span unsupported side lengths of up to 2.5 mm, and (c) a corrugated YSZ design with Si support showing an array of membranes.[65] Images used with permission.

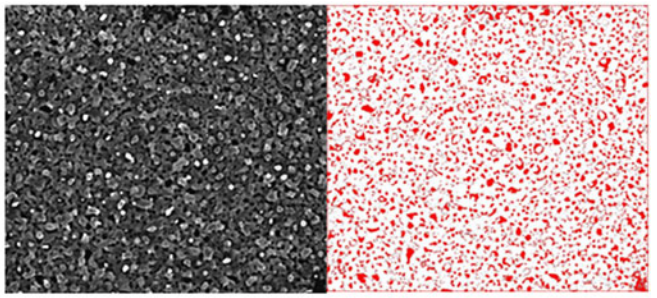
enables lower operating temperatures and reduces transport losses, as discussed earlier. There has been a significant effort in fabricating and testing such structures, some of which have been described in brief elsewhere.[55] Figure 8(a) shows a representative survey of the areal scaling of YSZ membranes that have been incorporated into TF-SOFC structures.[60,65,66,91,107] Theoretical limits on electrolyte thickness (h) reduction based on two distinct cases of electrode geometry describe the reduction of h in the context of electrode particle spacing (b), stating that $h < 300$ nm is not necessarily beneficial.[111] Nanoporous Pt electrodes, commonly used in TF-SOFCs, typically have particle spacing, and hence reaction sites, on the order of tens of nanometers as depicted in the micrograph shown in Fig. 8(b).[112] Linear reduction of Ohmic loss with electrolyte thickness is valid only when $h \gg b$.[111] Therefore, based on the nanoporous electrodes utilized in TF-SOFCs, the benefits of electrolyte thickness reduction certainly stretch below 300 nm. In fact, subsequent work reviewing progress on dimensionality reduction of ionic conducting materials points out the advantage of devices having $h \sim 150$ nm.[17] Figure 8(c) shows an example of experimental scaling of the maximum current density (and hence power density) as a function of electrolyte thickness, showing an exponential increase.[110] In addition, an ideal electrolyte area specific resistance (ASR) of 0.1 Ωcm^2 or less is desired for SOFCs.[113] At 500 °C using stable, nonexotic electrolyte materials such as YSZ and CGO membranes, ASRs of 0.08 and 0.04 Ωcm^2 have been reported.[50,112]

Initial design aspects for TF-SOFCs described mechanical buckling as a failure,[114,115] though a revised design space was later introduced,[116] and a plethora of experimental evidence indicates that buckling is a necessary element for self-supported ultrathin oxide components. In addition to the thin film electrolyte, an anode and cathode where oxidation and reduction take place, respectively, are required to complete the TF-SOFC. Besides their electrochemical functions, the electrodes must have adequate electrical conductivity to draw electrons from the device and into an external load. Figure 8(d) shows a schematic of the transport processes and test structure used in typical TF-SOFC experiments.[58] Utilizing thin electrolytes has pioneered operation temperatures ($T < 500$ °C) previously inaccessible with equivalent materials and thus, high performance oxide electrodes are scarce at present. Therefore, many of the initial investigations have utilized porous metals as both the anode and cathode due to high electrocatalytic activity and electronic conductivity. However, commonly used metal films such as Pt often

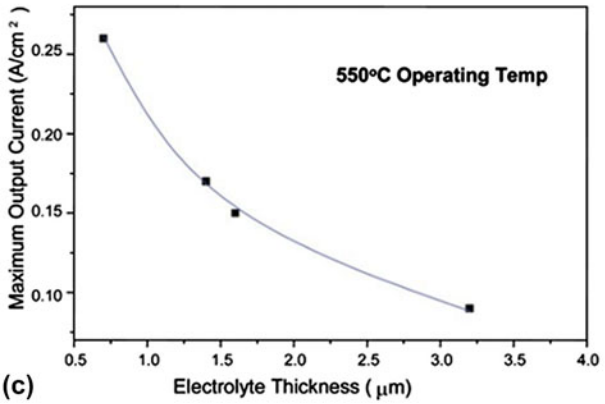
https://doi.org/10.1557/jmr.2013.301 Published online by Cambridge University Press

Membrane area (cm^2)	Output (mW)	Ref.
0.0001	0.035 at 500 °C	91
0.0001	0.134 at 500 °C	66
0.04	3 at 450 °C	65
0.25	0.25 at 500 °C	107
0.25	20 at 510 °C	60

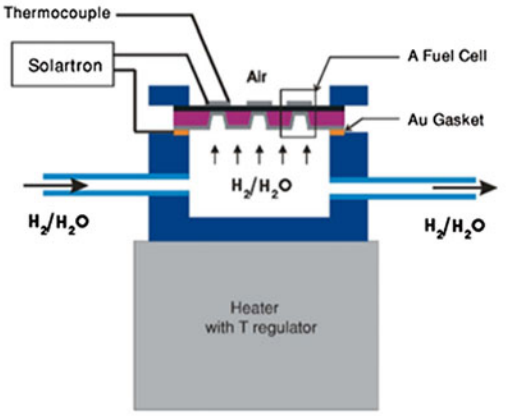
(a)



(b)



(c)



(d)

FIG. 8. (a) A survey of active area and total power output reported using free-standing YSZ membranes integrated into TF-SOFCs,[60,65,66,91,107] (b) a scanning electron microscope image and corresponding thresholded image showing the nanoporosity of Pt electrodes in TF-SOFCs, (c) the experimentally measured maximum current from a TF-SOFC as a function of electrolyte thickness,[110] (d) a test schematic of membrane structures utilized in TF-SOFC applications.[58] Images (c) and (d) used with permission.

suffer from coarsening and dewetting effects at elevated temperatures and under electrochemical perturbations,[117,118] which render the electrode microstructure of these proof-of-concept devices unstable.

A pristine membrane is essential for TF-SOFCs since the open circuit voltage (OCV) is determined by two factors; the thermodynamic redox potential of fuel/oxidant and adequate physical/electrical separation. The former is related to the catalytic activity of the electrodes and exact redox couple selected. For the most part, H_2 and air (21% O_2) have been used, which results in an OCV of approximately 1 V in the temperature range of interest (300 °C $< T <$ 500 °C) for the electrochemical reaction, $H_2 + \frac{1}{2}O_2 \rightarrow H_2O$. The latter is a macroscopic culmination of the previously described complexities in oxide membrane fabrication. A gas tight seal can only be realized if there are no microstructural defects, such as pinholes or microcracks, through the thickness of the self-supported membrane. Further, any electronic leakage reduces the OCV and thus the voltage efficiency of the TF-SOFC. Figure 9(a) shows a plot of OCV as a function of temperature for several YSZ thicknesses, indicating that even with an electrolyte of 27 nm, a near ideal potential is maintained.[112] In the case of materials possessing mixed valent cations and thus $0 < t_i < 1$, such as CGO, a percolative electronic path can emerge with critical compositions at the reducing interface.[50,120] OCVs have been shown to be stable over ranges of 10–50 h, indicating that the oxide membrane remains intact at high temperature under a chemical potential at these elevated temperatures.[50,112,119,121]

B. Electrode complexity and integration

A survey of the maximum power density of state-of-the-art TF-SOFCs utilizing Pt electrodes and YSZ membrane electrolytes is plotted in Fig. 9(b).[57,58,64,66,67,91,112,116] Power densities in excess of 1 W/cm^2 have been routinely achieved at temperatures around 500 °C using H_2 and air as the fuel and oxidant, respectively. Some current–voltage and current–power curves at various temperatures are shown for a planar YSZ-based TF-SOFC in Fig. 9(c).[112] Unlike high temperature SOFCs, there appears to be a significant activation loss in these devices. This is largely undesirable since a sizable overpotential (driving voltage) is necessary to mediate the oxygen reduction reaction (ORR)

https://doi.org/10.1557/jmr.2013.301 Published online by Cambridge University Press

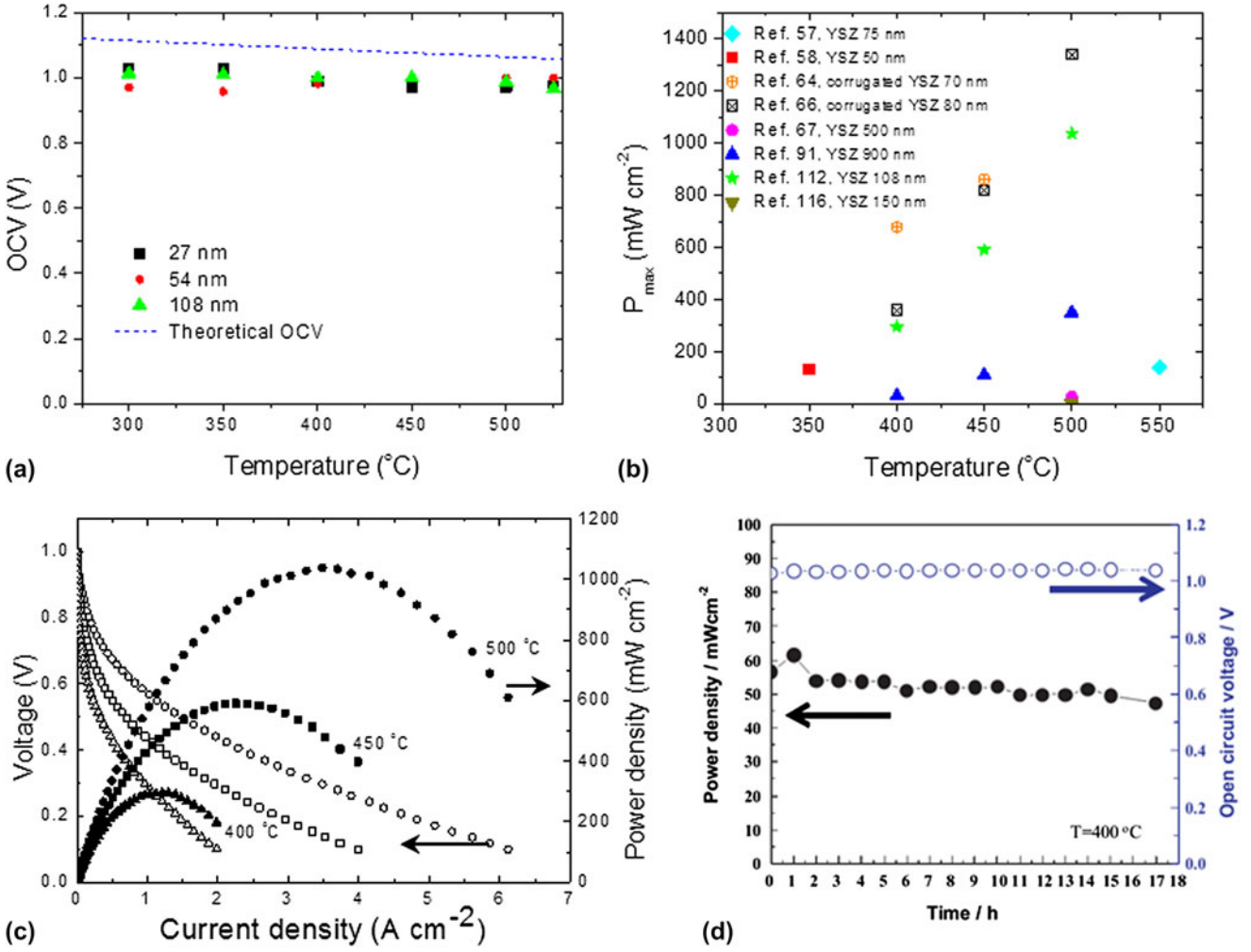


FIG. 9. (a) Pt/YSZ/Pt TF-SOFCs showing a near ideal OCV with varying electrolyte thickness using 5% H_2 as the fuel and air as the oxidant,[112] (b) state of the art power densities for Pt/YSZ/Pt TF-SOFCs using both planar and corrugated membranes with YSZ membranes,[57,58,64,66,67,91,112,116] (c) current–voltage and current–power characteristics of a Pt/YSZ/Pt TF-SOFC at several temperatures using a 108-nm YSZ membrane electrolyte,[112] and (d) an example of the temperature stability of performance and OCV of a Pt/YSZ/Pt TF-SOFC using a patterned Pt anode.[119] Image (d) used with permission.

on Pt, which has been a subject of intense research among the physical chemistry community in the context of proton exchange membrane fuel cells for years.[122] Typically oxide cathodes do not exhibit this loss, which serves as motivation for material researchers to develop a stable high performance oxide cathode suitable for this temperature regime.

As seen in Fig. 9(b), there is variation in the performance of the Pt/YSZ/Pt devices, in part due to electrolyte thickness and configuration differences but largely owing to the microstructural complexity of the electrodes at elevated temperature and reducing conditions.[112,121] Additionally, the method of current collection strongly influences the maximum power being extracted from the cell. A power density increase by a factor of 1.6 was recently realized by adding a denser metallic current collecting grid onto a $La_xSr_{1-x}Co_yO_3$ (LSC) cathode.[123] In the case of metal electrodes, only the triple phase boundaries, areas where the gaseous fuel, electrolyte, and electrode are in contact, are active reaction sites for oxidation and reduction. Consequently, engineering of the microstructure to create optimal porosity in the electrodes while maintaining an electrically interconnected network is of essence. However, as noted previously, the operational stability of such metallic electrodes is not at a desirable level.[112,121] Previous studies on Pt films on rigid substrates highlight the microstructural instability under TF-SOFC operating conditions,[117,118] though there has been success in utilizing the dewetting effect to form regular and stable patterned Pt.[124] Further, recent work on TF-SOFCs has shown that the microstructure of Pt electrodes can be stabilized when using an anodized aluminum oxide template, showing losses of only 10% in power density after 17 h of operation, highlighted in Fig. 9(d).[119] Nanosphere lithography is an alternative approach to

https://doi.org/10.1557/jmr.2013.301 Published online by Cambridge University Press

engineering regularly patterned metallic electrodes that have been shown to be morphologically stable at elevated temperatures.[125–127] However, the pattern density of such electrodes is far below what is necessary for high performance TF-SOFCs and thus may be limited to fundamental research similar to patterned complex oxide microelectrodes such as LSCF.[128] In cells exhibiting power densities over 1 W/cm^2, the anode triple phase boundary length per unit area was estimated to be 1,510,000 cm/cm^2 from thresholded scanning electron micrographs.[112] This is in the range of 800,000 cm/cm^2 calculated from surface reconstruction experiments of traditional SOFC electrodes after operation.[129,130] Therefore, the porosity, tortuosity, and interconnectivity of random networks appear much more viable than regular patterning experimentally conceivable at present.

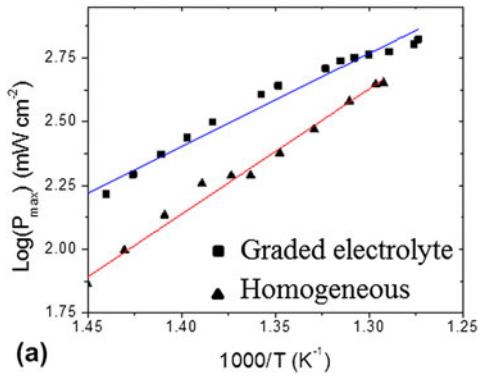
Efforts have been made to integrate complex oxide cathodes such as LSCF and $Ba_xSr_{1-x}Co_yFe_{1-y}O_3$ (BSCF) onto YSZ membranes with varying degrees of success, forming bilayer oxide heterostructure membranes with porous platinum anodes.[57,60,87,92,93,107] Integration of these layers requires thorough knowledge of the various stresses resulting from fabrication described in Sec. II. D. BSCF suffers from a parasitic reaction with YSZ even at TF-SOFC temperatures,[93] and is kinetically unstable over time at elevated temperature.[131,132] The power densities of LSCF/YSZ/Pt structures remain lower than that of Pt/YSZ/Pt counterparts but offer promise of the integration of dense oxide heterostructure membranes. As a proof of concept, LSCF/YSZ/LSCF membranes have been fabricated and survive thermomechanical stresses induced from fabrication and high temperature testing.[94] However, it should be noted that oxide electrodes containing Sr, such as LSC, LSCF, and BSCF may suffer from the long-term issue of Sr surface segregation.[133–136]

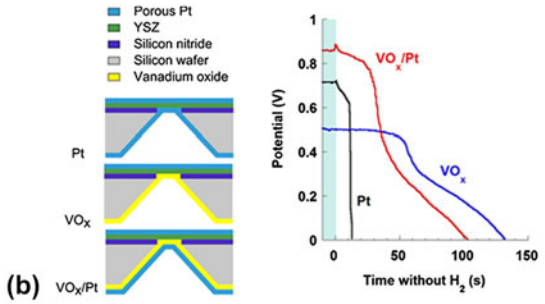
C. Novel capabilities of oxide membranes

The observation of low temperature protonic conduction in YSZ[137,138] and similar oxides such as $BaY_xZr_{1-x}O_3$ (BYZ) has led to TF-SOFCs with protons as the mobile ionic species.[8,139] Although the power densities reported in such systems is lower than what is shown in Fig. 9(b), proton-conducting ceramic membranes present opportunities in ultralow temperature (25 °C) power generation[138] and steam permeation reforming of hydrocarbons.[140] The challenges in designing oxide materials with chemical stability, ease of fabrication, and high protonic conductivity have been reviewed previously.[141] Of course, reduction of Ohmic transport loss through the oxide makes membrane structures appealing in this class of rapidly evolving materials.

Thin film processing and membrane structures offer unique advantages not possible with bulk systems. For example, low temperature processing assisted by photon irradiation has been shown to lead to desired crystalline oxide phases.[12,142] Furthermore, to overcome structural limitations of CGO membranes due to σ_e, oxide alloys of CGO–YSZ were fabricated by co-sputtering at temperatures as low as 25 °C.[50] This represents an enormous reduction in traditional processing temperatures in excess of 1300 °C needed to form solid solution mixtures of YSZ and CGO.[143,144] Tailoring of the electrolyte composition on the nanoscale is also possible when using bottom-up fabrication techniques. For example, superlattices of ALD-grown layers of Y_2O_3 and ZrO_2 have been shown to form YSZ after high temperature annealing, exhibiting enhanced transport properties.[145] Similarly, studies on superlattices of SiO_2 and CGO indicate that an apatite phase with high conductivity can be formed at the oxide interface.[146] Further, the addition of ALD surface layers (17.5 nm) of Y_2O_3-doped CeO_2 on YSZ has been shown to increase ORR activity and overall performance of TF-SOFCs.[147] An example of a compositionally graded electrolyte membrane that synergistically combines the mechanical stability of YSZ with higher σ_i of CGO has been demonstrated using a co-sputtering process with varying deposition rates.[120] It has recently been shown that CeO_2 possesses a highly electrocatalytic surface, comparable to that of bare metals.[148] Therefore, using a graded membrane could lead to additional catalytic activity at the electrolyte–electrode interface, in addition to enhanced σ_i. As shown in Fig. 10(a), when comparing the kinetic behavior, shown in an Arrhenius plot, of a compositionally graded electrolyte with a homogeneous YSZ electrolyte operating with methane (CH_4) as the fuel and air as the oxidant, there appears to be an advantage with the former.[120] The activation barrier to maximum power of the compositionally graded electrolyte was calculated to be 0.72 eV, whereas that of the homogeneous electrolyte was 0.97 eV.[120] Though this may be related to many factors, such as the surface energy contribution for metallic electrode spreading, the ability to create functionally graded structures for synergistic energy applications opens up a large design space for future materials. For reference, ionic transport in YSZ is typically characterized by an activation energy of ~1 eV.[5,23,30] Figure 10(b) shows an example of new device functionality in a TF-SOFC utilizing the mixed valence of vanadium oxide.[97] In this scheme, with several proposed mechanisms related to hydrogen storage, oxygen concentration differences, or fuel-less redox of V at the anode, the TF-SOFC acts as both an electrochemical energy conversion and storage device.[97] The key aspect of this work is demonstrating both fuel cell and battery characteristics in a single unique device. With practical application in mind, there have also been explorations into using abundant fuel sources such as CH_4 and natural gas with TF-SOFCs. Recent results are briefly summarized in Fig. 10(c).[112,149–152] However, long-term stability of electrodes using hydrocarbon fuels remains an open problem.[153–155]

https://doi.org/10.1557/jmr.2013.301 Published online by Cambridge University Press





Anode	Fuel	P_{max} (mW cm^{-2})	T (°C)	OCV (V)	Ref.
Pt	CH_4	95	440	0.86	112
Ru	CH_4	450	500	0.71	149
Pd	CH_4	385	550	0.77	150
Ru-CGO	CH_4	275	485	0.97	151
Ru	NG	800	530	0.95	152

(c)

FIG. 10. Novel abilities in thin film processing exhibited by (a) an Arrhenius plot of the maximum power density in TF-SOFCs with a compositionally graded (CGO–YSZ) and homogeneous YSZ electrolyte,[120,149] (b) vanadium oxide anodes exhibiting the unique capability of both energy conversion and storage by using a multivalent complex oxide electrode in a TF-SOFC,[97] and (c) a table summarizing the recent results of TF-SOFCs tested with fuels other than H_2.[112,149–152]. Figure (b) used with permission.

The integration of TF-SOFCs as a MEMS power system requires a wide-spanning collaborative effort. This ongoing journey has manifested itself in private ventures,[156] in addition to collaborative academic work.[157–159] An enclosed TF-SOFC system utilizing butane as fuel targeted for rapid recharging of mobile devices has been developed.[156] Similarly, fabrication of highly scalable square membranes with a metallic support grid using KOH processing has been shown.[60] In an effort to facilitate stacking, micromachined wafer scale gas flow channels in Si have been explored.[157] Researchers have also developed a battery replacement system with a thermally enclosed TF-SOFC power source.[158] To utilize a wider abundance of fuels, an integrated microfuel reformer has been recently investigated, showing butane conversion rates of up to 85%.[159] The path to commercialization will require the development of stable electrode materials, cost-effective manufacturing processes, fast start up times, ability to use widely available fuels such as natural gas, consideration of earth abundant materials, and most importantly continued investment of resources in the field of alternate energy.

IV. EMERGING RESEARCH DIRECTIONS IN TWO-DIMENSIONAL OXIDE MEMBRANES

Areas well-suited for study can be broadly categorized into (A) condensed matter science and (B) energy conversion technology, which we discuss briefly.

A. Condensed matter sciences and emergent phenomena

Complex oxide membranes can be utilized as a tunable experimental platform to probe fundamental limits of charge separation under various external perturbations, such as strain, electric field, partial pressure, and temperature. Studies on emergent transport in quasi-two-dimensional systems require intricate sample fabrication with geometrical conditions suitable for electrical measurement under external bias with negligible loss. This is of extraordinary relevance to avoiding artifacts in measurements (such as electron leakage currents). Film processing and device fabrication require great care since it is easy to create oxygen point defects during annealing steps, dry etching or ion beam-induced surface cleaning. Complex oxides are in part deemed "complex" due to the subtle interplay between the structure and the composition and the subsequent influence of electronic, magnetic, or electrochemical properties. For fundamental understanding of carrier transport and dimensionality effects in suspended membranes, it is therefore crucial to develop robust fabrication schemes.

Once such structures can be fabricated, oxide membranes create a powerful platform to probe dimensionality crossover; thereby answering questions pertaining to connections between intrinsic two-dimensional effects, many body correlations, gating in the presence of ionic liquids, and interfacial chemical phenomena. As described in Sec. I, the cross-over regime need not be down to atomic layers for complex oxides. Transport processes can often be elucidated by evaluating an externally controllable variable; therefore, robust complex oxide membrane structures offer a potential experimental platform to explore some of the cutting edge problems in condensed matter especially under strong electric fields. Initial studies on conduction in suspended VO_2 membranes show a drastic

https://doi.org/10.1557/jmr.2013.301 Published online by Cambridge University Press

shift in the metal–insulator transition temperature due to stress relaxation in the self-supported membrane, which could be of relevance for tuning operating temperatures for low power switching or sensor devices and understanding elementary mechanisms of the material response to electric fields in ionic liquid environments.[11,95] We anticipate that these methods could be of great interest in investigating correlated electron phenomena in suspended/confined structures and will see growth in the coming years.

B. Energy conversion technologies

Membrane-based gas separation technologies have long touted the benefits of thickness reduction for higher ionic throughput in selectively permeable oxide materials. Mixed conducting complex oxides, $0 < t_i < 1$, such as LSCF and BSCF have applications in industrial processes for conversion of CH_4.[160–162] Several schematic examples of procedures possible are shown in Fig. 11.[163–165] Compared to steam-reforming, $CH_4 + H_2O \rightarrow CO + 3H_2$, the partial oxidation process, $CH_4 + \frac{1}{2}O_2 \rightarrow 2H_2 + CO$, is advantageous due to higher throughput and exothermic nature, rendering an external power source unnecessary.[166] Using several mixed conducting membranes in series can allow simultaneous generation and separation of H_2 and N_2, as shown in Fig. 11(a).[163] Oxide membranes having $t_i = 1$ have their use in the production of high purity oxygen from air[165] and generating H_2 with an external current applied.[164] The operating principle of the latter is similar to SOFCs described in Sec. II but utilized in regenerative mode to produce H_2 from H_2O via electrolysis. To be economically feasible, these processes require large volumes of feedstock and hence high geometric membrane area. Additionally, high gas pressures on the order of hundreds of kilopascals are used in many cases to increase overall system conversion efficiency. Therefore, challenges in the synthesis of industrial scale thin film oxide membranes that can operate at high temperature and system pressure remain open and constitute a worthy research topic. Further, detailed understanding of the mechanics in ultrathin membranes under varying partial pressures and high ambient pressures warrants diligent attention.

An opportunity exists to engineer such membranes into energy conversion and storage devices having ultra-low weight and hence high specific energies, assuming one can also scale the accompanying balance of plant accordingly. Such intriguing opportunities will find application in future generations of advanced electronics, sensors, and bioinspired design of autonomous vehicles that can exploit membranes. Moreover, as the field of robotics is rapidly advancing, small scale power sources simply do not

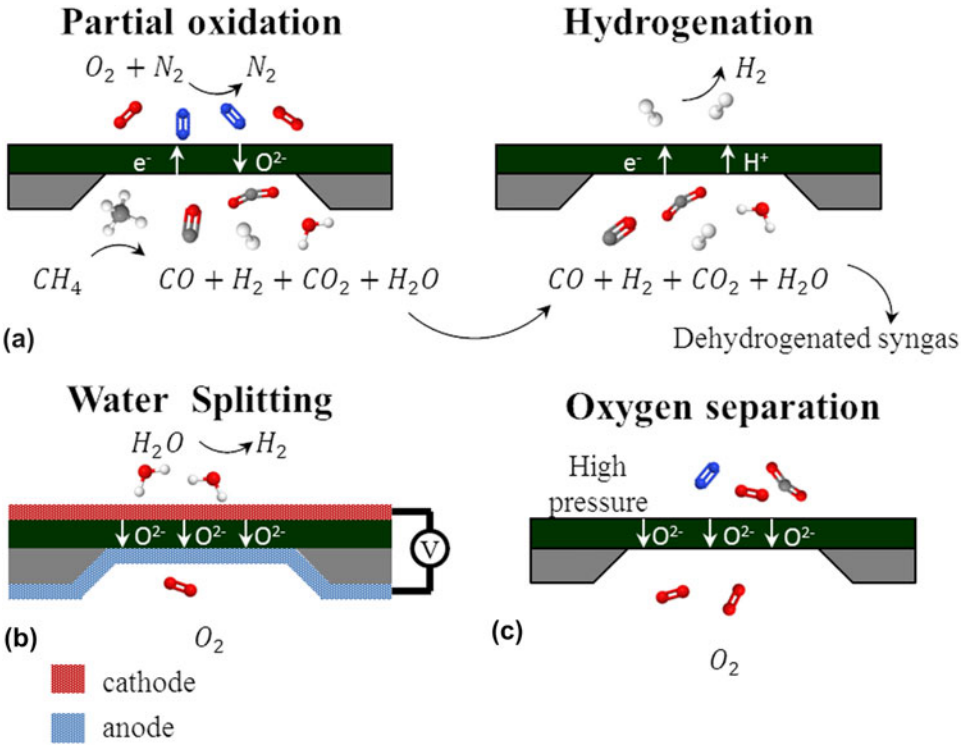


FIG. 11. Opportunities to use oxide membranes in gas separation and processing applications; (a) a two-step process illustrating the production of syngas and subsequent generation and separation of H_2 and N_2 using a partial oxidation then hydrogenation step with mixed conducting oxide membranes,[163] (b) splitting water by electrolysis using an oxygen conducting membrane to separate H_2 and O_2,[164] and (c) creation of ultra-high purity O_2 by filtering air or other potential gases.

https://doi.org/10.1557/jmr.2013.301 Published online by Cambridge University Press

exist at present to meet the desired capabilities for state of the art systems.[167] The extraordinary needs in autonomous systems that can operate in land, air, or sea in complex environments will be a major driving force for research in mobile energy sources in the coming years. Similarly, storing and converting energy for MEMS using a micropower supply has long been an overarching goal.[168]

In summary, we have highlighted research areas related to suspended complex oxide membranes, both films and heterostructures. Understanding the influence of processing and film stresses is vital for fabricating robust structures that can be electrically interrogated under a range of temperatures, oxygen pressures, and electric fields. The unique opportunities and preliminary results discussed in this review suggest that there is a great deal of scientific and engineering frontiers ahead, having implications in energy technology and condensed matter material sciences.

ACKNOWLEDGMENT

KK was supported by the Department of Defense through the NDSEG fellowship.

REFERENCES

1. I. Elmi, S. Zampolli, E. Cozzani, F. Mancarella, and G.C. Cardinali: Development of ultra-low-power consumption MOX sensors with ppb-level VOC detection capabilities for emerging applications. *Sens. Actuators, B* **135**(1), 342 (2008).
2. M.D. Nguyen, H.N. Vu, D.H.A. Blank, and G. Rijnders: Epitaxial Pb(Zr, Ti)O_3 thin films for a MEMS application. *Adv. Nat. Sci.: Nanosci. Nanotechnol.* **2**(1), 015005 (2011).
3. A. Kossoy, A.I. Frenkel, Y. Feldman, E. Wachtel, A. Milner, and I. Lubomirsky: The origin of elastic anomalies in thin films of oxygen deficient ceria, CeO_{2-x}. *Solid State Ionics* **181**(33–34), 1473 (2010).
4. C. Ko, K. Kerman, and S. Ramanathan: Ultra-thin film solid oxide fuel cells utilizing un-doped nanostructured zirconia electrolytes. *J. Power Sources* **213**(0), 343 (2012).
5. I. Garbayo, A. Tarancón, J. Santiso, F. Peiró, E. Alarcón-Lladó, A. Cavallaro, I. Gràcia, C. Cané, and N. Sabaté: Electrical characterization of thermomechanically stable YSZ membranes for micro solid oxide fuel cells applications. *Solid State Ionics* **181**(5–7), 322 (2010).
6. S. Rey-Mermet and P. Muralt: Solid oxide fuel cell membranes supported by nickel grid anode. *Solid State Ionics* **179**(27–32), 1497 (2008).
7. M. Greenberg, E. Wachtel, I. Lubomirsky, J. Fleig, and J. Maier: Elasticity of solids with a large concentration of point defects. *Adv. Funct. Mater.* **16**(1), 48 (2006).
8. J.H. Shim, J.S. Park, J. An, T.M. Gür, S. Kang, and F.B. Prinz: Intermediate-temperature ceramic fuel cells with thin film yttrium-doped barium zirconate electrolytes. *Chem. Mater.* **21**(14), 3290 (2009).
9. J. He, P. Kanjanaboos, N.L. Frazer, A. Weis, X-M. Lin, and H.M. Jaeger: Fabrication and mechanical properties of large-scale freestanding nanoparticle membranes. *Small* **6**(13), 1449 (2010).
10. A. Dong, J. Chen, P.M. Vora, J.M. Kikkawa, and C.B. Murray: Binary nanocrystal superlattice membranes self-assembled at the liquid-air interface. *Nature* **466**(7305), 474 (2010).
11. J.S. Sim, Y. Zhou, and S. Ramanathan: Suspended sub-50 nm vanadium dioxide membrane transistors: Fabrication and ionic liquid gating studies. *Nanoscale* **4**(22), 7056 (2012).
12. M. Tsuchiya, B-K. Lai, A.C. Johnson, and S. Ramanathan: Photon-assisted synthesis of ultra-thin yttria-doped zirconia membranes: Structure, variable temperature conductivity and micro-fuel cell devices. *J. Power Sources* **195**(4), 994 (2010).
13. R.A. De Souza: The formation of equilibrium space-charge zones at grain boundaries in the perovskite oxide $SrTiO_3$. *Phys. Chem. Chem. Phys.* **11**(43), 9939 (2009).
14. J. Maier: Defect chemistry and ionic conductivity in thin films. *Solid State Ionics* **23**(1–2), 59 (1987).
15. H.L. Tuller: Ionic conduction in nanocrystalline materials. *Solid State Ionics* **131**(1–2), 143 (2000).
16. S.M. Sze and K.K. Ng: *Physics of Semiconductor Devices* (John Wiley & Sons, Hoboken, NJ, 2006).
17. H.L. Tuller, S.J. Litzelman, and W. Jung: Micro-ionics: Next generation power sources. *Phys. Chem. Chem. Phys.* **11**(17), 3023 (2009).
18. I. Kosacki, C.M. Rouleau, P.F. Becher, J. Bentley, and D.H. Lowndes: Nanoscale effects on the ionic conductivity in highly textured YSZ thin films. *Solid State Ionics* **176**(13–14), 1319 (2005).
19. B. Li, J. Zhang, T. Kaspar, V. Shutthanandan, R.C. Ewing, and J. Lian: Multilayered YSZ/GZO films with greatly enhanced ionic conduction for low temperature solid oxide fuel cells. *Phys. Chem. Chem. Phys.* **15**(4), 1296 (2013).
20. A. Karthikeyan, C-L. Chang, and S. Ramanathan: High temperature conductivity studies on nanoscale yttria-doped zirconia thin films and size effects. *Appl. Phys. Lett.* **89**(18), 183116 (2006).
21. M. Sillassen, P. Eklund, N. Pryds, E. Johnson, U. Helmersson, and J. Bøttiger: Low-temperature superionic conductivity in strained yttria-stabilized zirconia. *Adv. Funct. Mater.* **20**(13), 2071 (2010).
22. M. Gerstl, G. Friedbacher, F. Kubel, H. Hutter, and J. Fleig: The relevance of interfaces for oxide ion transport in yttria stabilized zirconia (YSZ) thin films. *Phys. Chem. Chem. Phys.* **15**(4), 1097 (2013).
23. X. Guo: Can we achieve significantly higher ionic conductivity in nanostructured zirconia? *Scr. Mater.* **65**(2), 96 (2011).
24. H-R. Kim, J-C. Kim, K-R. Lee, H-I. Ji, H-W. Lee, J-H. Lee, and J-W. Son: 'Illusional' nano-size effect due to artifacts of in-plane conductivity measurements of ultra-thin films. *Phys. Chem. Chem. Phys.* **13**(13), 6133 (2011).
25. E. Navickas, M. Gerstl, G. Friedbacher, F. Kubel, and J. Fleig: Measurement of the across-plane conductivity of YSZ thin films on silicon. *Solid State Ionics* **211**(0), 58 (2012).
26. S. Kim and J. Maier: On the conductivity mechanism of nanocrystalline ceria. *J. Electrochem. Soc.* **149**(10), J73 (2002).
27. X. Guo and Y. Ding: Grain boundary space charge effect in zirconia: Experimental evidence. *J. Electrochem. Soc.* **151**(1), J1 (2004).
28. A. Tschöpe: Grain size-dependent electrical conductivity of polycrystalline cerium oxide II: Space charge model. *Solid State Ionics* **139**(3–4), 267 (2001).
29. O.J. Durá, M.A. López de la Torre, L. Vázquez, J. Chaboy, R. Boada, and A. Rivera-Calzada, J. Santamaria, and C. Leon: Ionic conductivity of nanocrystalline yttria-stabilized zirconia: Grain boundary and size effects. *Phys. Rev. B* **81**(18), 184301 (2010).
30. I. Kosacki, T. Suzuki, V. Petrovsky, and H.U. Anderson: Electrical conductivity of nanocrystalline ceria and zirconia thin films. *Solid State Ionics* **136–137**(0), 1225 (2000).
31. H. Huang, T.M. Gur, Y. Saito, and F. Prinz: High ionic conductivity in ultrathin nanocrystalline gadolinia-doped ceria films. *Appl. Phys. Lett.* **89**(14), 143107 (2006).

https://doi.org/10.1557/jmr.2013.301 Published online by Cambridge University Press

32. A. Karthikeyan, M. Tsuchiya, C-L. Chang, and S. Ramanathan: Tunable electrical conductivity in nanoscale Gd-doped ceria thin films. *Appl. Phys. Lett.* **90**(26), 263108 (2007).
33. S.K.R.S. Sankaranarayanan and S. Ramanathan: Interface proximity effects on ionic conductivity in nanoscale oxide-ion conducting yttria stabilized zirconia: An atomistic simulation study. *J. Chem. Phys.* **134**(6), 064703 (2011).
34. W. Jung, J.L. Hertz, and H.L. Tuller: Enhanced ionic conductivity and phase meta-stability of nano-sized thin film yttria-doped zirconia (YDZ). *Acta Mater.* **57**(5), 1399 (2009).
35. S.C. Singhal and K. Kendall: *High-temperature Solid Oxide Fuel Cells: Fundamentals, Design and Applications: Fundamentals, Design and Applications* (Elsevier Inc., New York, 2003).
36. R.P. O'Hayre, S-W Cha, W. Colella, and F.B. Prinz: *Fuel Cell Fundamentals* (John Wiley & Sons, Hoboken, NJ, 2006).
37. A. Kushima and B. Yildiz: Oxygen ion diffusivity in strained yttria stabilized zirconia: Where is the fastest strain? *J. Mater. Chem.* **20**(23), 4809 (2010).
38. M.J.D. Rushton, A. Chroneos, S.J. Skinner, J.A. Kilner, and R.W. Grimes: Effect of strain on the oxygen diffusion in yttria and gadolinia co-doped ceria. *Solid State Ionics* **230**(0), 37 (2013).
39. J. Jiang, X. Hu, W. Shen, C. Ni, and J.L. Hertz: Improved ionic conductivity in strained yttria-stabilized zirconia thin films. *Appl. Phys. Lett.* **102**(14), 143901 (2013).
40. J.L.M. Rupp: Ionic diffusion as a matter of lattice-strain for electroceramic thin films. *Solid State Ionics* **207**(0), 1 (2012).
41. J.L.M. Rupp, B. Scherrer, A.S. Harvey, and L.J. Gauckler: Crystallization and grain growth kinetics for precipitation-based ceramics: A case study on amorphous ceria thin films from spray pyrolysis. *Adv. Funct. Mater.* **19**(17), 2790 (2009).
42. B. Scherrer, S. Heiroth, R. Hafner, J. Martynczuk, A. Bieberle-Hütter, J.L.M. Rupp, and L.J. Gauckler: Crystallization and microstructure of yttria-stabilized-zirconia thin films deposited by spray pyrolysis. *Adv. Funct. Mater.* **21**(20), 3967 (2011).
43. Y. Lvov, F. Essler, and G. Decher: Combination of polycation/polyanion self-assembly and Langmuir-Blodgett transfer for the construction of superlattice films. *J. Phys. Chem.* **97**(51), 13773 (1993).
44. G.G. Roberts: An applied science perspective of Langmuir-Blodgett films. *Adv. Phys.* **34**(4), 475 (1985).
45. L.J. Cote, F. Kim, and J. Huang: Langmuir–Blodgett assembly of graphite oxide single layers. *J. Am. Chem. Soc.* **131**(3), 1043 (2008).
46. G. Eda, G. Fanchini, and M. Chhowalla: Large-area ultrathin films of reduced graphene oxide as a transparent and flexible electronic material. *Nat. Nanotechnol.* **3**(5), 270 (2008).
47. W. Cheng, M.J. Campolongo, S.J. Tan, and D. Luo: Freestanding ultrathin nano-membranes via self-assembly. *Nano Today* **4**(6), 482 (2009).
48. J. Will, A. Mitterdorfer, C. Kleinlogel, D. Perednis, and L.J. Gauckler: Fabrication of thin electrolytes for second-generation solid oxide fuel cells. *Solid State Ionics* **131**(1–2), 79 (2000).
49. L.R. Pederson, P. Singh, and X.D. Zhou: Application of vacuum deposition methods to solid oxide fuel cells. *Vacuum* **80**(10), 1066 (2006).
50. K. Kerman, B-K. Lai, and S. Ramanathan: Free standing oxide alloy electrolytes for low temperature thin film solid oxide fuel cells. *J. Power Sources* **202**(0), 120 (2012).
51. K.R. Williams and R.S. Muller: Etch rates for micromachining processing. *J. Microelectromech. Syst.* **5**(4), 256 (1996).
52. K.R. Williams, K. Gupta, and M. Wasilik: Etch rates for micromachining processing: Part II. *J. Microelectromech. Syst.* **12**(6), 761 (2003).
53. C. Liu, V.B. Mungurwadi, and A.V. Nandi: *Foundations of MEMS* (Prentice Hall, Saddle River, NJ, 2011).
54. J. Korvink and O. Paul: *MEMS: A Practical Guide to Design, Analysis and Applications* (William Andrew Inc., Norwich, NY, 2005).
55. A. Evans, A. Bieberle-Hütter, J.L.M. Rupp, and L.J. Gauckler: Review on microfabricated micro-solid oxide fuel cell membranes. *J. Power Sources* **194**(1), 119 (2009).
56. C.D. Baertsch, K.F. Jensen, J.L. Hertz, H.L. Tuller, S.T. Vengallatore, S.M. Spearing, and M.A. Schmidt: Fabrication and structural characterization of self-supporting electrolyte membranes for a micro solid-oxide fuel cell. *J. Mater. Res.* **19**(9), 2604 (2004).
57. A.C. Johnson, B-K. Lai, H. Xiong, and S. Ramanathan: An experimental investigation into micro-fabricated solid oxide fuel cells with ultra-thin $La_{0.6}Sr_{0.4}Co_{0.8}Fe_{0.2}O_3$ cathodes and yttria-doped zirconia electrolyte films. *J. Power Sources* **186**(2), 252 (2009).
58. H. Huang, M. Nakamura, P. Su, R. Fasching, Y. Saito, and F.B. Prinz: High-performance ultrathin solid oxide fuel cells for low-temperature operation. *J. Electrochem. Soc.* **154**(1), B20 (2007).
59. S.J. Litzelman, J.L. Hertz, W. Jung, and H.L. Tuller: Opportunities and challenges in materials development for thin film solid oxide fuel cells. *Fuel Cells* **8**, 294 (2008).
60. M. Tsuchiya, B-K. Lai, and S. Ramanathan: Scalable nanostructured membranes for solid-oxide fuel cells. *Nat. Nanotechnol.* **6**(5), 282 (2011).
61. H. Seidel, L. Csepregi, A. Heuberger, and H. Baumgärtel: Anisotropic etching of crystalline silicon in alkaline solutions: I. Orientation dependence and behavior of passivation layers. *J. Electrochem. Soc.* **137**(11), 3612 (1990).
62. J.L.M. Rupp, U.P. Muecke, P.C. Nalam, and L.J. Gauckler: Wet-etching of precipitation-based thin film microstructures for micro-solid oxide fuel cells. *J. Power Sources* **195**(9), 2669 (2010).
63. A. Bieberle-Hütter, P. Reinhard, J.L.M. Rupp, and L.J. Gauckler: The impact of etching during microfabrication on the microstructure and the electrical conductivity of gadolinia-doped ceria thin films. *J. Power Sources* **196**(15), 6070 (2011).
64. P-C. Su, C-C. Chao, J.H. Shim, R. Fasching, and F.B. Prinz: Solid oxide fuel cell with corrugated thin film electrolyte. *Nano Lett.* **8**(8), 2289 (2008).
65. P-C. Su and F.B. Prinz: Nanoscale membrane electrolyte array for solid oxide fuel cells. *Electrochem. Commun.* **16**(1), 77 (2012).
66. C-C. Chao, C-M. Hsu, Y. Cui, and F.B. Prinz: Improved solid oxide fuel cell performance with nanostructured electrolytes. *ACS Nano* **5**(7), 5692 (2011).
67. U.P. Muecke, D. Beckel, A. Bernard, A. Bieberle-Hütter, S. Graf, A. Infortuna, P. Müller, J.L.M. Rupp, J. Schneider, and L.J. Gauckler: Micro solid oxide fuel cells on glass ceramic substrates. *Adv. Funct. Mater.* **18**(20), 3158 (2008).
68. J. Hertz, A. Rothschild, and H. Tuller: Highly enhanced electrochemical performance of silicon-free platinum–yttria stabilized zirconia interfaces. *J. Electroceram.* **22**(4), 428 (2009).
69. B. Scherrer, A. Rossi, J. Martynczuk, M.D. Rossell, A. Bieberle-Hütter, J.L.M. Rupp, R. Erni, and L.J. Gauckler: Impact of substrate material and annealing conditions on the microstructure and chemistry of yttria-stabilized-zirconia thin films. *J. Power Sources* **196**(18), 7372 (2011).
70. S. Timoshenko: *Theory of Elasticity* (McGraw-Hill, United States, 1934).
71. L.L.D. Landau, E.M. Lifshitz, A.M. Kosevitch, and L.P. Pitaevskiĭ: *Theory of Elasticity*, Vol. **7** (Butterworth-Heinemann, Waltham, MA, 1986).
72. V. Ziebart, O. Paul, and H. Baltes: Strongly buckled square micromachined membranes. *J. Microelectromech. Syst.* **8**(4), 423 (1999).
73. E. Cerda and L. Mahadevan: Geometry and physics of wrinkling. *Phys. Rev. Lett.* **90**(7), 074302 (2003).

https://doi.org/10.1557/jmr.2013.301 Published online by Cambridge University Press

74. T. Tallinen, J.A. Astrom, and J. Timonen: The effect of plasticity in crumpling of thin sheets. *Nat. Mater.* **8**(1), 25 (2009).
75. L.B. Freund and S. Suresh: *Thin Film Materials: Stress, Defect Formation and Surface Evolution* (Cambridge University Press, Cambridge, UK, 2003).
76. K. Kerman, T. Tallinen, S. Ramanathan, and L. Mahadevan: Elastic configurations of self-supported oxide membranes for fuel cells. *J. Power Sources* **222**(0), 359 (2013).
77. J.H. Cheon, P.S. Shankar, and J.P. Singh: Influence of processing methods on residual stress evolution in coated conductors. *Supercond. Sci. Technol.* **18**(1), 142 (2005).
78. A. Evans, M. Prestat, R. Tölke, M.V.F. Schlupp, L.J. Gauckler, Y. Safa, T. Hocker, J. Courbat, D. Briand, N.F. de Rooij, and D. Courty: Residual stress and buckling patterns of free-standing yttria-stabilized-zirconia membranes fabricated by pulsed laser deposition. *Fuel Cells* **12**(4), 614 (2012).
79. J. Carneiro, V. Teixeira, A. Portinha, F. Vaz, and J. Ferreira: A real time scale measurement of residual stress evolution during coating deposition using electric extensometry. *Rev. Adv. Mater. Sci.* **7**, 32 (2004).
80. D.J. Quinn, B. Wardle, and S.M. Spearing: Residual stress and microstructure of as-deposited and annealed, sputtered yttria-stabilized zirconia thin films. *J. Mater. Res.* **23**(3), 609 (2008).
81. Q. Xiao, H. He, S. Shao, J. Shao, and Z. Fan: Influences of deposition rate and oxygen partial pressure on residual stress and microstructure of YSZ thin films. *Thin Solid Films* **517**(15), 4295 (2009).
82. M. Ohring: *Materials Science of Thin Films* (Academic Press, San Diego, CA, 2001).
83. F. Spaepen: Interfaces and stresses in thin films. *Acta Mater.* **48**(1), 31 (2000).
84. K.V.L.V. Narayanachari and S. Raghavan: Stress and texture development during sputtering of yttria, zirconia, and yttria stabilized zirconia films on Si substrates. *J. Appl. Phys.* **112**(7), 074910 (2012).
85. R.W. Knoll and E.R. Bradley: Correlation between the stress and microstructure in bias-sputtered ZrO_2-Y_2O_3 films. *Thin Solid Films* **117**(3), 201 (1984).
86. A. Infortuna, A.S. Harvey, and L.J. Gauckler: Microstructures of CGO and YSZ thin films by pulsed laser deposition. *Adv. Funct. Mater.* **18**(1), 127 (2008).
87. B.K. Lai, H. Xiong, M. Tsuchiya, A.C. Johnson, and S. Ramanathan: Microstructure and microfabrication considerations for self-supported on-chip ultra-thin micro-solid oxide fuel cell membranes. *Fuel Cells* **9**(5), 699 (2009).
88. S. Heiroth, R. Frison, J.L.M. Rupp, T. Lippert, E.J. Barthazy Meier, E. Müller Gubler, M. Döbeli, K. Conder, A. Wokaun, and L.J. Gauckler: Crystallization and grain growth characteristics of yttria-stabilized zirconia thin films grown by pulsed laser deposition. *Solid State Ionics* **191**(1), 12 (2011).
89. I. Garbayo, G. Dezanneau, C. Bogicevic, J. Santiso, I. Gràcia, N. Sabaté, and A. Tarancón: Pinhole-free YSZ self-supported membranes for micro solid oxide fuel cell applications. *Solid State Ionics* **216**(0), 64 (2012).
90. S. Rey-Mermet, Y. Yan, C. Sandu, G. Deng, and P. Muralt: Nanoporous YSZ film in electrolyte membrane of micro-solid oxide fuel cell. *Thin Solid Films* **518**(16), 4743 (2010).
91. C-W. Kwon, J-W. Son, J-H. Lee, H-M. Kim, H-W. Lee, and K-B. Kim: High-performance micro-solid oxide fuel cells fabricated on nanoporous anodic aluminum oxide templates. *Adv. Funct. Mater.* **21**(6), 1154 (2011).
92. B-K. Lai, K. Kerman, and S. Ramanathan: On the role of ultra-thin oxide cathode synthesis on the functionality of micro-solid oxide fuel cells: Structure, stress engineering and in situ observation of fuel cell membranes during operation. *J. Power Sources* **195**(16), 5185 (2010).
93. K. Kerman, B-K. Lai, and S. Ramanathan: Thin film nanocrystalline $Ba_{0.5}Sr_{0.5}Co_{0.8}Fe_{0.2}O_3$: Synthesis, conductivity, and micro-solid oxide fuel cells. *J. Power Sources* **196**(15), 6214 (2011).
94. B-K. Lai, K. Kerman, and S. Ramanathan: Nanostructured $La_{0.6}Sr_{0.4}Co_{0.8}Fe_{0.2}O_3$/$Y_{0.08}Zr_{0.92}O_{1.96}$/$La_{0.6}Sr_{0.4}Co_{0.8}Fe_{0.2}O_3$ (LSCF/YSZ/LSCF) symmetric thin film solid oxide fuel cells. *J. Power Sources* **196**(4), 1826 (2011).
95. V. Balakrishnan, C. Ko, and S. Ramanathan: In situ studies on twinning and cracking proximal to insulator–metal transition in self-supported VO_2/Si_3N_4 membranes. *J. Mater. Res.* **27**(11), 1476 (2012).
96. P.J. Fillingham: Domain structure and twinning in crystals of vanadium dioxide. *J. Appl. Phys.* **38**(12), 4823 (1967).
97. Q. Van Overmeere, K. Kerman, and S. Ramanathan: Energy storage in ultrathin solid oxide fuel cells. *Nano Lett.* **12**(7), 3756 (2012).
98. I. Lubomirsky: Practical applications of the chemical strain effect in ionic and mixed conductors. *Monatsh. Chem.* **140**(9), 1025 (2009).
99. K.L. Duncan, Y. Wang, S.R. Bishop, F. Ebrahimi, and E.D. Wachsman: Role of point defects in the physical properties of fluorite oxides. *J. Am. Ceram. Soc.* **89**(10), 3162 (2006).
100. S.R. Bishop, K.L. Duncan, and E.D. Wachsman: Thermo-chemical expansion in strontium-doped lanthanum cobalt iron oxide. *J. Am. Ceram. Soc.* **93**(12), 4115 (2010).
101. D. Marrocchelli, S.R. Bishop, H.L. Tuller, and B. Yildiz: Understanding chemical expansion in non-stoichiometric oxides: Ceria and zirconia case studies. *Adv. Funct. Mater.* **22**(9), 1958 (2012).
102. S. Bishop, D. Marrocchelli, W. Fang, K. Amezawa, K. Yashiro, and G. Watson: Reducing the chemical expansion coefficient in ceria by addition of zirconia. *Energy Environ. Sci.* **6**(4), 1142–1146 (2013).
103. H.L. Tuller and S.R. Bishop: Point defects in oxides: Tailoring materials through defect engineering. *Ann. Rev. Mater. Res.* **41**, 369 (2011).
104. J.P. Nair, E. Wachtel, I. Lubomirsky, J. Fleig, and J. Maier: Anomalous expansion of CeO_2 nanocrystalline membranes. *Adv. Mater.* **15**(24), 2077 (2003).
105. S.B. Adler: Chemical expansivity of electrochemical ceramics. *J. Am. Ceram. Soc.* **84**(9), 2117 (2001).
106. S.R. Bishop, K.L. Duncan, and E.D. Wachsman: Surface and bulk oxygen non-stoichiometry and bulk chemical expansion in gadolinium-doped cerium oxide. *Acta Mater.* **57**(12), 3596 (2009).
107. A.C. Johnson, A. Baclig, D.V. Harburg, B-K. Lai, and S. Ramanathan: Fabrication and electrochemical performance of thin-film solid oxide fuel cells with large area nanostructured membranes. *J. Power Sources* **195**(4), 1149 (2010).
108. S.A. Barnett: A new solid oxide fuel cell design based on thin film electrolytes. *Energy* **15**(1), 1 (1990).
109. L.C. De Jonghe, C.P. Jacobson, and S.J. Visco: Supported electrolyte thin film synthesis of solid oxide fuel cells. *Ann. Rev. Mater. Res.* **33**(1), 169 (2003).
110. A. Ignatiev, X. Chen, N. Wu, Z. Lu, and L. Smith: Nanostructured thin solid oxide fuel cells with high power density. *Dalton Trans.* (40), 5501 (2008).
111. J. Fleig, H.L. Tuller, and J. Maier: Electrodes and electrolytes in micro-SOFCs: A discussion of geometrical constraints. *Solid State Ionics* **174**(1–4), 261 (2004).
112. K. Kerman, B-K. Lai, and S. Ramanathan: Pt/$Y_{0.16}Zr_{0.84}O_{1.92}$/Pt thin film solid oxide fuel cells: Electrode microstructure and stability considerations. *J. Power Sources* **196**(5), 2608 (2011).
113. B.C.H. Steele and A. Heinzel: Materials for fuel-cell technologies. *Nature* **414**(6861), 345 (2001).
114. V.T. Srikar, K.T. Turner, T.Y. Andrew Ie, and S.M. Spearing: Structural design considerations for micromachined solid-oxide fuel cells. *J. Power Sources* **125**(1), 62 (2004).

https://doi.org/10.1557/jmr.2013.301 Published online by Cambridge University Press

115. Y. Tang, K. Stanley, J. Wu, D. Ghosh, and J. Zhang: Design consideration of micro thin film solid-oxide fuel cells. *J. Micromech. Microeng.* **15**(9), S185 (2005).
116. N. Yamamoto, D.J. Quinn, N. Wicks, J.L. Hertz, J. Cui, H.L. Tuller, and B.L. Wardle: Nonlinear thermomechanical design of microfabricated thin plate devices in the post-buckling regime. *J. Micromech. Microeng.* **20**(3), 035027 (2010).
117. E. Mutoro, S. Günther, B. Luerßen, I. Valov, and J. Janek: Electrode activation and degradation: Morphology changes of platinum electrodes on YSZ during electrochemical polarisation. *Solid State Ionics* **179**(33–34), 1835 (2008).
118. H. Galinski, T. Ryll, P. Elser, J.L.M. Rupp, A. Bieberle-Hütter, and L.J. Gauckler: Agglomeration of Pt thin films on dielectric substrates. *Phys. Rev. B* **82**(23), 235415 (2010).
119. C-W. Kwon, J-I. Lee, K-B. Kim, H-W. Lee, J-H. Lee, and J-W. Son: The thermomechanical stability of micro-solid oxide fuel cells fabricated on anodized aluminum oxide membranes. *J. Power Sources* **210**(0), 178 (2012).
120. K. Kerman, B-K. Lai, and S. Ramanathan: Nanoscale compositionally graded thin-film electrolyte membranes for low-temperature solid oxide fuel cells. *Adv. Energy Mater.* **2**(6), 655 (2012).
121. X. Wang, H. Huang, T. Holme, X. Tian, and F.B. Prinz: Thermal stabilities of nanoporous metallic electrodes at elevated temperatures. *J. Power Sources* **175**(1), 75 (2008).
122. N. Marković, T. Schmidt, V. Stamenković, and P. Ross: Oxygen reduction reaction on Pt and Pt bimetallic surfaces: A selective review. *Fuel Cells* **1**(2), 105 (2001).
123. H-S. Noh, J. Hwang, K. Yoon, B-K. Kim, H-W. Lee, J-H. Lee, and J-W. Son: Optimization of current collection to reduce the lateral conduction loss of thin-film-processed cathodes. *J. Power Sources* **230**(0), 109 (2013).
124. N. Baumann, E. Mutoro, and J. Janek: Porous model type electrodes by induced dewetting of thin Pt films on YSZ substrates. *Solid State Ionics* **181**(1–2), 7 (2010).
125. E.C. Brown, S.K. Wilke, D.A. Boyd, D.G. Goodwin, and S.M. Haile: Polymer sphere lithography for solid oxide fuel cells: A route to functional, well-defined electrode structures. *J. Mater. Chem.* **20**(11), 2190 (2010).
126. Y.B. Kim, C-M. Hsu, S.T. Connor, T.M. Gür, Y. Cui, and F.B. Prinz: Nanopore patterned Pt array electrodes for triple phase boundary study in low temperature SOFC. *J. Electrochem. Soc.* **157**(9), B1269 (2010).
127. A.Y. Lin and P.C. McIntyre: Morphological stability of mesoporous Pt thin films deposited via nanosphere lithography on YSZ. *Electrochem. Solid-State Lett.* **14**(10), B96 (2011).
128. N.J. Simrick, J.A. Kilner, A. Atkinson, J.L.M. Rupp, T.M. Ryll, A. Bieberle-Hütter, H. Galinski, and L.J. Gauckler: Microfabrication of patterned LSCF thin-film cathodes with gold current collectors. *Solid State Ionics* **192**(1), 619 (2011).
129. J.R. Wilson, W. Kobsiriphat, R. Mendoza, H-Y. Chen, J.M. Hiller, D.J. Miller, K. Thornton, P.W. Voorhees, S.B. Adler, and S.A. Barnett: Three-dimensional reconstruction of a solid-oxide fuel-cell anode. *Nat. Mater.* **5**(7), 541 (2006).
130. J.R. Wilson, M. Gameiro, K. Mischaikow, W. Kalies, P.W. Voorhees, and S.A. Barnett: Three-dimensional analysis of solid oxide fuel cell Ni-YSZ anode interconnectivity. *Microsc. Microanal.* **15**(1), 71 (2009).
131. D.N. Mueller, R.A. De Souza, T.E. Weirich, D. Roehrens, J. Mayer, and M. Martin: A kinetic study of the decomposition of the cubic perovskite-type oxide $Ba_xSr_{1-x}Co_{0.8}Fe_{0.2}O_3$-[small delta] (BSCF) (x = 0.1 and 0.5). *Phys. Chem. Chem. Phys.* **12**(35), 10320 (2010).
132. C. Niedrig, S. Taufall, M. Burriel, W. Menesklou, S.F. Wagner, S. Baumann, and E. Ivers-Tiffée: Thermal stability of the cubic phase in $Ba_{0.5}Sr_{0.5}Co_{0.8}Fe_{0.2}O_{3-\delta}$ (BSCF)1. *Solid State Ionics* **197**(1), 25 (2011).
133. S.R. Bishop, K.L. Duncan, and E.D. Wachsman: Surface and bulk defect equilibria in strontium-doped lanthanum cobalt iron oxide. *J. Electrochem. Soc.* **156**(10), B1242 (2009).
134. S. Fearn, J. Rossiny, and J. Kilner: SIMS artifacts in the near surface depth profiling of oxygen conducting ceramics. *Solid State Ionics* **179**(21–26), 811 (2008).
135. Y. Chen, W. Jung, Z. Cai, J.J. Kim, H.L. Tuller, and B. Yildiz: Impact of Sr segregation on the electronic structure and oxygen reduction activity of $SrTi_{1-x}Fe_xO_3$ surfaces. *Energy Environ. Sci.* **5**(7), 7979 (2012).
136. A-K. Huber, M. Falk, M. Rohnke, B. Luer, L. Gregoratti, M. Amati, and J. Janek: In situ study of electrochemical activation and surface segregation of the SOFC electrode material $La_{0.75}Sr_{0.25}Cr_{0.5}Mn_{0.5}O_3$ =/− δ *Phys. Chem. Chem. Phys.* **14**(2), 751 (2012).
137. H.J. Avila-Paredes, E. Barrera-Calva, H.U. Anderson, R.A. De Souza, M. Martin, Z.A. Munir, and S. Kim: Room-temperature protonic conduction in nanocrystalline films of yttria-stabilized zirconia. *J. Mater. Chem.* **20**(30), 6235 (2010).
138. S. Kim, U. Anselmi-Tamburini, H.J. Park, M. Martin, and Z.A. Munir: Unprecedented room-temperature electrical power generation using nanoscale fluorite-structured oxide electrolytes. *Adv. Mater.* **20**(3), 556 (2008).
139. D. Pergolesi, E. Fabbri, and E. Traversa: Chemically stable anode-supported solid oxide fuel cells based on Y-doped barium zirconate thin films having improved performance. *Electrochem. Commun.* **12**(7), 977 (2010).
140. W.G. Coors: Steam reforming, and water-gas shift by steam permeation in a protonic ceramic fuel cell. *J. Electrochem. Soc.* **151**(7), A994 (2004).
141. E. Fabbri, D. Pergolesi, and E. Traversa: Materials challenges toward proton-conducting oxide fuel cells: A critical review. *Chem. Soc. Rev.* **39**(11), 4355 (2010).
142. A. Podpirka, B. Viswanath, and S. Ramanathan: Active low temperature oxidation as a route to minimize electrode–oxide interface reactions in nanoscale capacitors. *J. Appl. Phys.* **108**(2), 024106 (2010).
143. M. Price, J. Dong, X. Gu, S.A. Speakman, E.A. Payzant, and T.M. Nenoff: Formation of YSZ–SDC solid solution in a nanocrystalline heterophase system and its effect on the electrical conductivity. *J. Am. Ceram. Soc.* **88**(7), 1812 (2005).
144. G.A. Tompsett, N.M. Sammes, and O. Yamamoto: Ceria–yttria-stabilized zirconia composite ceramic systems for applications as low-temperature electrolytes. *J. Am. Ceram. Soc.* **80**(12), 3181 (1997).
145. C.N. Ginestra, R. Sreenivasan, A. Karthikeyan, S. Ramanathan, and P.C. McIntyre: Atomic layer deposition of Y_2O_3/ZrO_2 nanolaminates: A route to ultrathin solid-state electrolyte membranes. *Electrochem. Solid-State Lett.* **10**(10), B161 (2007).
146. A. Karthikeyan, M. Tsuchiya, and S. Ramanathan: Apatite-phase synthesis from interdiffusion in doped CeO_2–SiO_2 thin-film superlattices and in situ conductivity studies. *Electrochem. Solid-State Lett.* **11**(11), K101 (2008).
147. Z. Fan, J. An, A. Iancu, and F.B. Prinz: Thickness effects of yttria-doped ceria interlayers on solid oxide fuel cells. *J. Power Sources* **218**(0), 187 (2012).
148. W.C. Chueh, Y. Hao, W. Jung, and S.M. Haile: High electrochemical activity of the oxide phase in model ceria–Pt and ceria–Ni composite anodes. *Nat. Mater.* **11**(2), 155 (2012).
149. Y. Takagi, B-K. Lai, K. Kerman, and S. Ramanathan: Low temperature thin film solid oxide fuel cells with nanoporous ruthenium anodes for direct methane operation. *Energy Environ. Sci.* **4**(9), 3473 (2011).

https://doi.org/10.1557/jmr.2013.301 Published online by Cambridge University Press

150. B-K. Lai, K. Kerman, and S. Ramanathan: Methane-fueled thin film micro-solid oxide fuel cells with nanoporous palladium anodes. *J. Power Sources* **196**(15), 6299 (2011).
151. Y. Takagi, S. Adam, and S. Ramanathan: Nanostructured ruthenium – gadolinia-doped ceria composite anodes for thin film solid oxide fuel cells. *J. Power Sources* **217**(0), 543 (2012).
152. Y. Takagi, K. Kerman, C. Ko, and S. Ramanathan: Operational characteristics of thin film solid oxide fuel cells with ruthenium anode in natural gas. *J. Power Sources* **243**(0), 1 (2013).
153. A. Atkinson, S. Barnett, R.J. Gorte, J. Irvine, A.J. McEvoy, M. Mogensen, S.C. Singhal, and J. Vohs: Advanced anodes for high-temperature fuel cells. *Nat. Mater.* **3**(1), 17 (2004).
154. R.J. Gorte, S. Park, J.M. Vohs, and C. Wang: Anodes for direct oxidation of dry hydrocarbons in a solid-oxide fuel cell. *Adv. Mater.* **12**(19), 1465 (2000).
155. M. Mogensen and K. Kammer: Conversion of hydrocarbons in solid oxide fuel cells. *Ann. Rev. Mater. Res.* **33**(1), 321 (2003).
156. S.B. Schaevitz: Powering the wireless world with MEMS. *Proc. SPIE* **8248**, 824802 (2012).
157. B-K. Lai, A.C. Johnson, M. Tsuchiya, and S. Ramanathan: Towards wafer-scale fabrication and 3D integration of micro-solid oxide fuel cells for portable energy. *Proc. SPIE* **7679**, 767916 (2010).
158. A. Bieberle-Hütter, D. Beckel, A. Infortuna, U.P. Muecke, J.L.M. Rupp, L.J. Gauckler, S. Rey-Mermet, P. Muralt, N.R. Bieri, N. Hotz, M.J. Stutz, D. Poulikakos, P. Heeb, P. Müller, A. Bernard, R. Gmür, and T. Hocker: A micro-solid oxide fuel cell system as battery replacement. *J. Power Sources* **177**(1), 123 (2008).
159. A. Bieberle-Hutter, A.J. Santis-Alvarez, B. Jiang, P. Heeb, T. Maeder, M. Nabavi, D. Poulikakos, P. Niedermann, A. Dommann, P. Muralt, A. Bernard, and L.J. Gauckler: Syngas generation from n-butane with an integrated MEMS assembly for gas processing in micro-solid oxide fuel cell systems. *Lab Chip* **12**(22), 4894 (2012).
160. J. Zaman and A. Chakma: Inorganic membrane reactors. *J. Membr. Sci.* **92**(1), 1 (1994).
161. R.W. Baker: Future directions of membrane gas separation technology. *Ind. Eng. Chem. Res.* **41**(6), 1393 (2002).
162. U. Balachandran, B. Ma, P. Maiya, R. Mieville, J. Dusek, J. Picciolo, J. Guan, S. Dorris, and M. Liu: Development of mixed-conducting oxides for gas separation. *Solid State Ionics* **108**(1), 363 (1998).
163. T. Norby and Y. Larring: Mixed hydrogen ion–electronic conductors for hydrogen permeable membranes. *Solid State Ionics* **136–137**(0), 139 (2000).
164. M.A. Laguna-Bercero: Recent advances in high temperature electrolysis using solid oxide fuel cells: A review. *J. Power Sources* **203**(0), 4 (2012).
165. P.N. Dyer, R.E. Richards, S.L. Russek, and D.M. Taylor: Ion transport membrane technology for oxygen separation and syngas production. *Solid State Ionics* **134**(1–2), 21 (2000).
166. C-Y. Tsai, A.G. Dixon, W.R. Moser, and Y.H. Ma: Dense perovskite membrane reactors for partial oxidation of methane to syngas. *AIChE J.* **43**(S11), 2741 (1997).
167. R.J. Wood, B. Finio, M. Karpelson, N.O. Pérez-Arancibia, P. Sreetharan, and J.P. Whitney: Challenges for micro-scale flapping-wing micro air vehicles. *Proc. SPIE* **8373**, 83731J (2012).
168. P.B. Koeneman, I.J. Busch-Vishniac, and K.L. Wood: Feasibility of micro power supplies for MEMS. *J. Microelectromech. Syst.* **6**(4), 355 (1997).

https://doi.org/10.1557/jmr.2013.301 Published online by Cambridge University Press